NASA CONTRACTOR
REPORT

NASA CR-150237

(NASA-CR-150237) PROTON-INDUCED RADIOACTIVITY IN NaI (Tl) SCINTILLATION DETECTORS Interim Report (Teledyne Brown Engineering) 69 p HC A04/MF A01 CSCL 18H

N77-23906

Unclas
G3/72 29064

PROTON-INDUCED RADIOACTIVITY IN NaI (Tℓ) SCINTILLATION DETECTORS

By G. J. Fishman
Teledyne Brown Engineering
Huntsville, Alabama 35807

Interim Report

April 1977

MAY 1977
RECEIVED
NASA STI FACILITY
INPUT BRANCH

Prepared for

NASA-GEORGE C. MARSHALL SPACE FLIGHT CENTER
Marshall Space Flight Center, Alabama 35812

TECHNICAL REPORT STANDARD TITLE PAGE

1. REPORT NO.	2. GOVERNMENT ACCESSION NO.	3 RECIPIENT'S CATALOG NO.
NASA CR-150237		

4 TITLE AND SUBTITLE	5. REPORT DATE
Proton-Induced Radioactivity in NaI(Tℓ) Scintillation Detectors	April 1977
	6 PERFORMING ORGANIZATION CODE

7 AUTHOR(S)	8 PERFORMING ORGANIZATION REPORT #
G. J. Fishman	

9. PERFORMING ORGANIZATION NAME AND ADDRESS	10. WORK UNIT NO.
Teledyne Brown Engineering Huntsville, Alabama 35807	11. CONTRACT OR GRANT NO. NAS8-26342
	13. TYPE OF REPORT & PERIOD COVERED Contractor Report
12. SPONSORING AGENCY NAME AND ADDRESS National Aeronautics and Space Administration Washington, D. C. 20546	14. SPONSORING AGENCY CODE

15 SUPPLEMENTARY NOTES

Prepared under the technical monitorship of the Nuclear and Plasma Physics Division, Space Sciences Laboratory, NASA/Marshall Space Flight Center

16. ABSTRACT

Radioactivity induced by protons in sodium iodide scintillation crystals has been calculated and directly measured. These data are useful in determining trapped radiation and cosmic-ray-induced, background-counting rates in space-borne detectors.

17. KEY WORDS	18. DISTRIBUTION STATEMENT
	Unclassified – Unlimited Ray V. Hembree for Charles A. Lundquist Director, Space Sciences Laboratory

19 SECURITY CLASSIF. (of this report)	20. SECURITY CLASSIF. (of this page)	21 NO. OF PAGES	22 PRICE
Unclassified	Unclassified	69	NTIS

MSFC - Form 3292 (Rev December 1972) For sale by National Technical Information Service, Springfield, Virginia 22151

TABLE OF CONTENTS

		Page
INTRODUCTION		1
CALCULATIONS		6
EXPERIMENT		16
SUMMARY AND CONCLUSIONS		22
REFERENCES		23
APPENDIX A.	NaI SPALLATION YIELDS	A-1
APPENDIX B.	600-MeV PROTON IRRADIATION SPECTRA OF NaI(Tℓ)	B-1
APPENDIX C.	TIME DECAY CURVES FOR 600-MeV PROTON IRRADIATED NaI(Tℓ)	C-1

LIST OF ILLUSTRATIONS

Figure	Title	Page
1	Proton Flux Contours for $E_p > 5$ MeV	2
2	Proton Energy Spectrum for h = 720 km, i = 30 degrees	3
3	Primary Galactic and Solar Cosmic-Ray Spectra	4
4	Iodine Spallation Yields at 1 GeV	7
5	Iodine Spallation Yields, 0.3 to 3.0 GeV	8
6	Sodium Spallation Yields, 0.3 to 3.0 GeV	9
7	Half-Life Distribution of Iodine Spallation Products	13
8	Energy Spectra Taken After 600 MeV Proton Irradiation	17
9	Induced Radioactivity Decay Profiles	19
10	Calculated and Measured Induced Radioactivity in a NaI(Tl) Crystal	20
B-1	Background Spectrum, SREL Measurements	B-3
B-2	Background Spectrum, MSFC Measurements	B-4
B-3	Spectrum Number 1	B-5
B-4	Spectrum Number 2	B-6
B-5	Spectrum Number 3	B-7
B-6	Spectrum Number 4	B-8
B-7	Spectrum Number 5	B-9
B-8	Spectrum Number 6	B-10

LIST OF ILLUSTRATIONS (Concluded)

Figure	Title	Page
B-9	Spectrum Number 7	B-11
B-10	Spectrum Number 8	B-12
B-11	Spectrum Number 9	B-13
B-12	Spectrum Number 10	B-14
C-1	Counting Rate as a Function of Time After Irradiation, Range 0.15 to 0.25 MeV	C-2
C-2	Counting Rate as a Function of Time After Irradiation, Range 0.25 to 0.40 MeV	C-3
C-3	Counting Rate as a Function of Time After Irradiation, Range 0.4 to 0.6 MeV	C-4
C-4	Counting Rate as a Function of Time After Irradiation, Range 0.6 to 1.0 MeV	C-5
C-5	Counting Rate as a Function of Time After Irradiation, Range 1 to 2 MeV	C-6
C-6	Counting Rate as a Function of Time After Irradiation, Range 2 to 3 MeV	C-7

LIST OF SYMBOLS

A	Atomic number
d	Day
E	Energy (detected count)
E_e'	e-folding energy
F_c	Induced counting rate
F_p	Inducing particle flux
f_i	Fraction of nuclear interactions
f_r	Fraction of products which are radioactive
f_t	Fraction of radioactive decays within an indicated time interval
h	Hour
j	Nucleus subscript
m	Minute
mb	millibarn = 10^{-27} cm^2
m_c	Multiplicity factor
N_o	Avagodro's number
t	Time
X	Mass thickness
σ	Cross section
$T_{\frac{1}{2}}$	Half-life
125 m	Isomeric state of isotope 125

INTRODUCTION

Proton-induced radioactivity of scintillation detectors is an important source of background-counting rate whenever these detectors are used in a space environment. In addition to the ever-present primary cosmic-rays, for spacecraft in Earth orbit, the trapped proton radiation adds considerably to the total proton flux. For orbits of low altitude and medium inclination, the largest fraction of the proton flux is received in the region of the South Atlantic Anomaly. Figure 1 shows the flux contours for protons with energies greater than 5 MeV at an altitude of 600 kilometers (Ref. 1). Figure 2 gives the proton energy spectrum averaged over 24 hours for an orbit at an altitude of 720 kilometers and an inclination of 30 degrees (Ref. 2). Figure 3 gives the primary cosmic-ray spectrum near the Earth.

Radioactivity induced in spacecraft scintillation detectors was first recognized and analyzed by Peterson on his OSO I experiment (Ref. 3). The analysis of data from the Russian gamma-ray experiments on the Cosmos 135 and Cosmos 163 spacecraft has included corrections for the radioactivity induced by passage through the region of the South Atlantic Anomaly, although the details of these corrections have not been given (Ref. 4). Dyer and Morfill (Ref. 5) have calculated the induced radioactivity in CsI(Tℓ) by the same general method used in the present report and have compared these calculations to radioactivity induced by 155-MeV protons. This energy is representative of that of nuclear-interacting trapped protons. Their measurements are used in a study of the anticipated background radiation on the UK-5 celestial gamma-ray experiment. The data contained within the present report has been used to determine the effect of cosmic-ray-induced radioactivity on diffuse celestial gamma-ray measurements (Ref. 6).

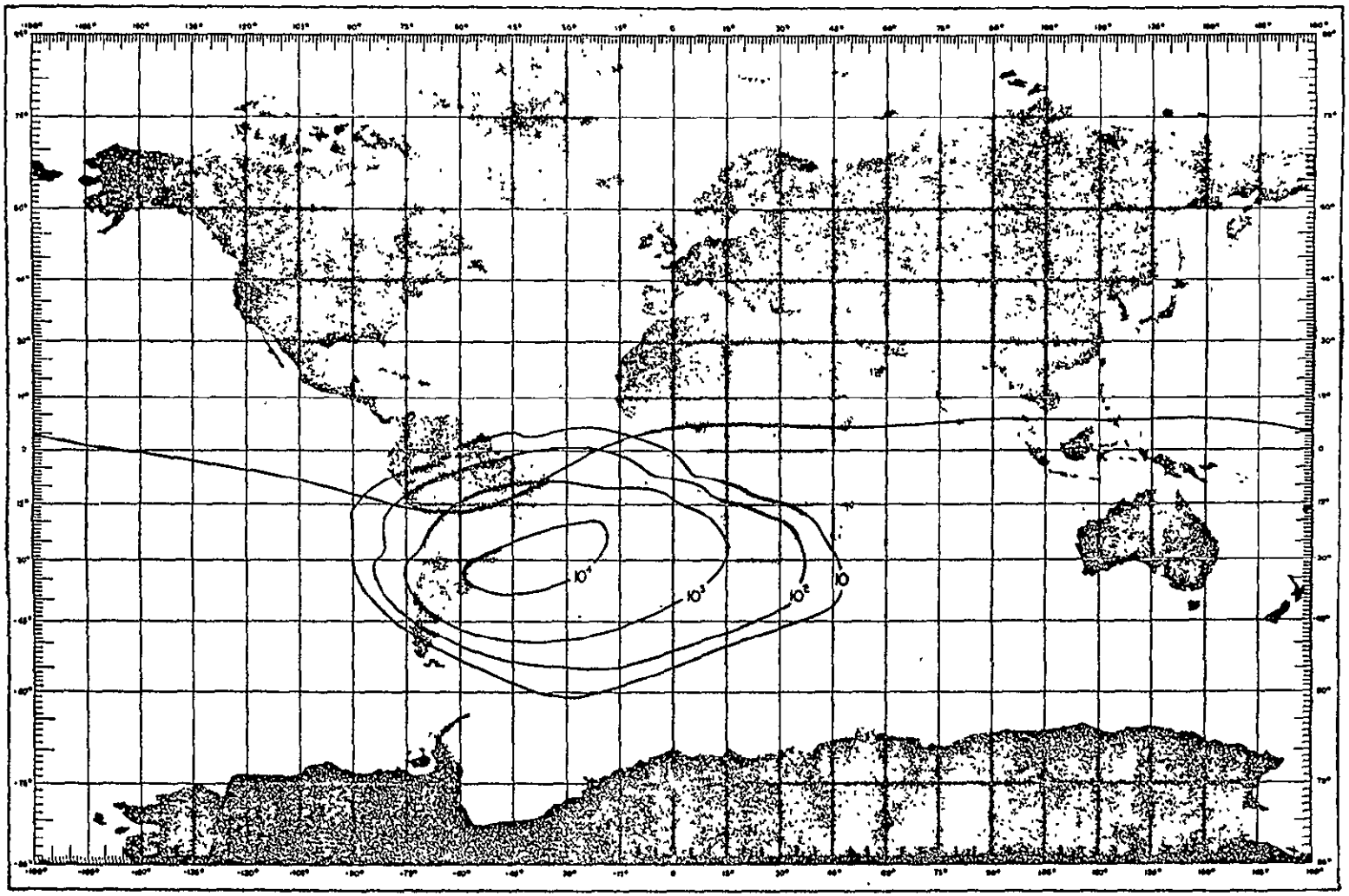

FIGURE 1. PROTON FLUX CONTOURS FOR E_p > 5 MeV

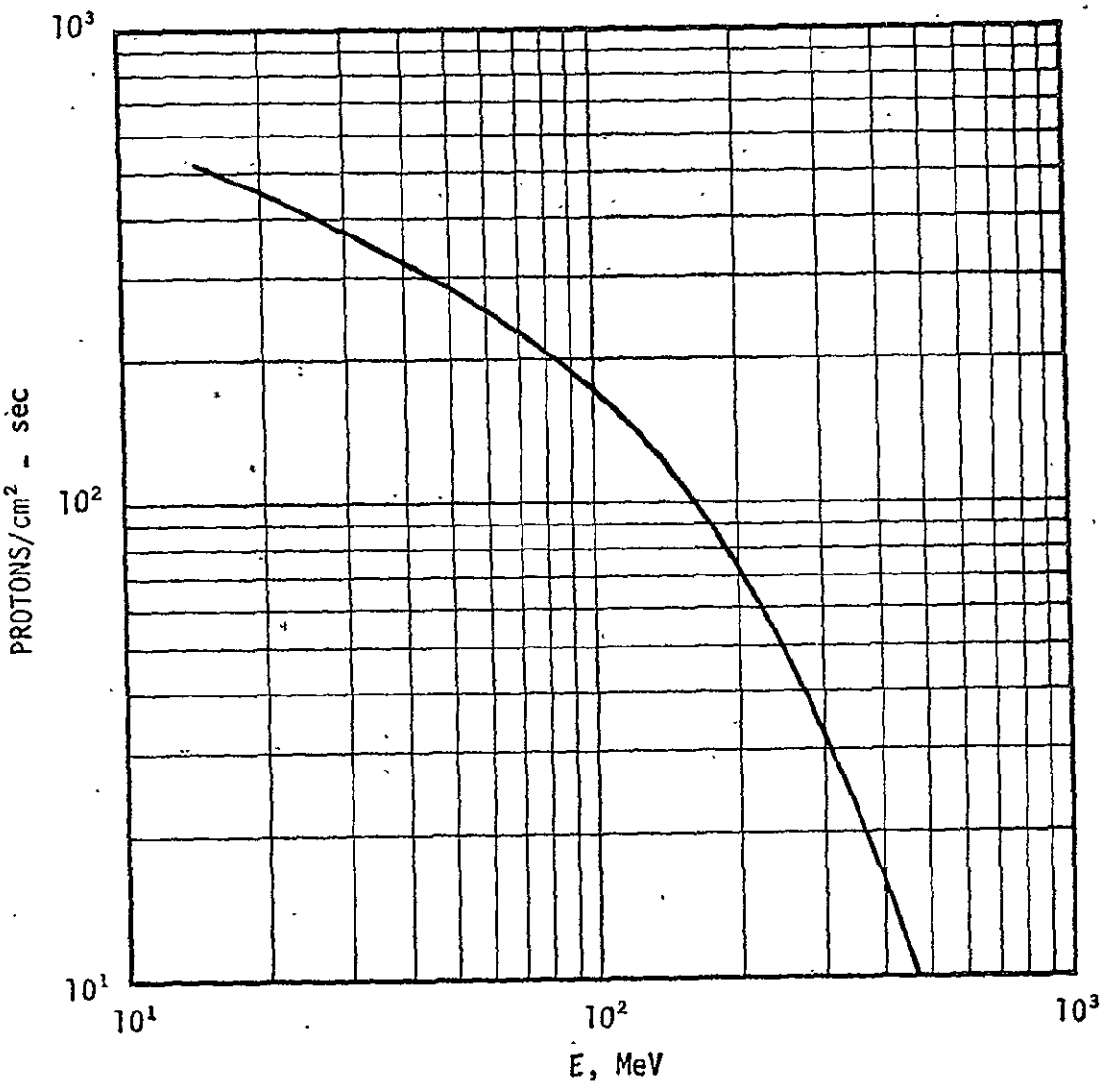

FIGURE 2. PROTON ENERGY SPECTRUM FOR h = 720 km, i = 30 degrees

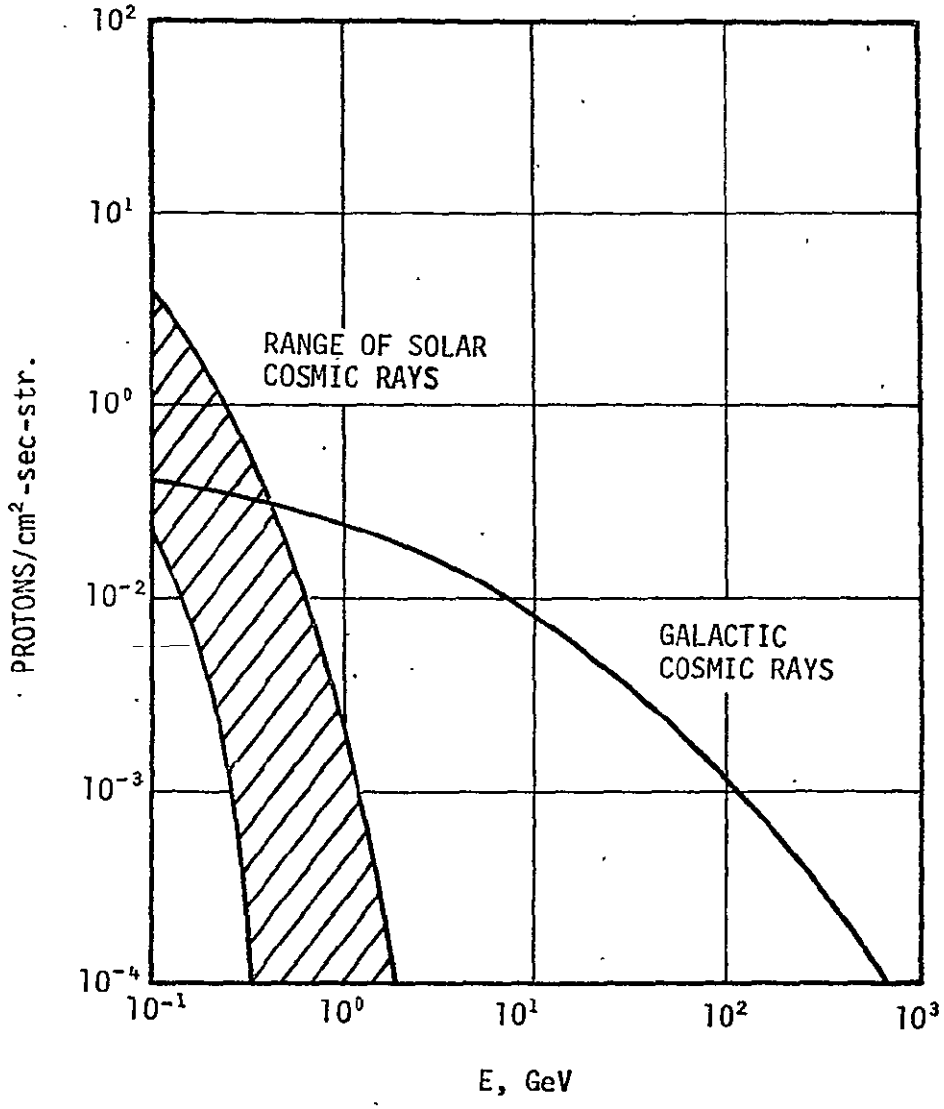

FIGURE 3. PRIMARY GALACTIC AND SOLAR COSMIC-RAY SPECTRA

To deduce the amount of radioactivity and its energy and time decay spectrum induced in scintillation detectors by protons, both an analytical approach and an experimental approach were undertaken. The analytical approach consisted of calculations of spallation yields and a study of the nuclear properties of the spallation products. The experimental approach was to irradiate a scintillation detector with high-energy protons and directly observe the counts resulting from the decay of induced radioactivity. Both approaches are limited in their estimation of the radioactivity induced in a true space environment. However, within errors, both estimates were in agreement and may prove useful in design and data reduction applications for space-borne experiments using scintillation detectors.

Portions of this report were published in a paper entitled "Cosmic-Ray Effects on Diffuse Gamma-Ray Measurements" (Ref. 6) and were presented at the Joint Meeting of the American Physical Society, Cosmic Physics Division and the American Astronomical Society, High Energy Astrophysics Division in San Juan, Puerto Rico, on December 3, 1971.

CALCULATIONS

Calculations of spallation yields were made for protons interacting with sodium iodide at energies above 100 MeV using the semi-empirical formulae derived by Rudstam (Ref. 7). These formulae give the cross section for spallation production within a factor of three over a wide range of atomic mass numbers and incident proton energies. The output of the program used to calculate the spallation production cross sections for protons incident on Na^{23} and I^{127} targets is given in Appendix A. Each output group represents a different product element, and a matrix of cross sections is presented as a function of isotope number and interaction energy. Several qualitative features are apparent from the data. These features (listed below) are direct results of the basic Rudstam formulae (Ref. 7):

- The peak cross section for each element is close to to the valley of beta stability for that element.
- At higher energies, the isotope production distribution is broader (cross sections fall off less rapidly) than at lower energies.
- The element production falls off exponentially with the difference in atomic number from the target element.
- The above fall-off is much more rapid at lower interaction energies.

The output data are presented in pictorial form in Figures 4, 5, and 6. Each of these figures represents a portion of the chart of nuclides (Ref. 8) in which the isotopes shown have a production cross section greater than that indicated on the figure at various energies.

ORIGINAL PAGE IS
OF POOR QUALITY

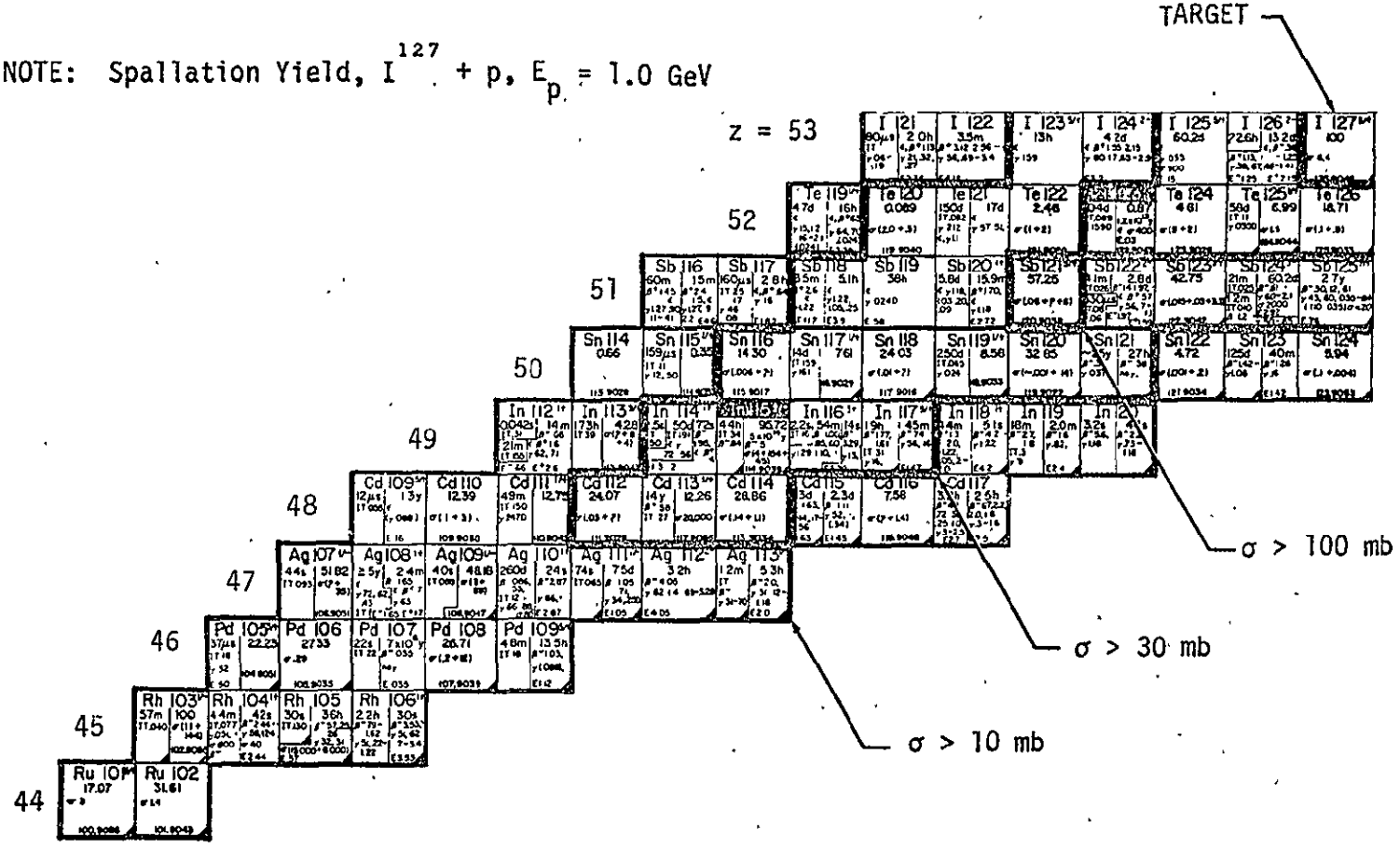

FIGURE 4. IODINE SPALLATION YIELDS AT 1 GeV

NOTE: IODINE SPALLATION PRODUCTS WITH σ > 10 mb; σ_t = 1,260 mb

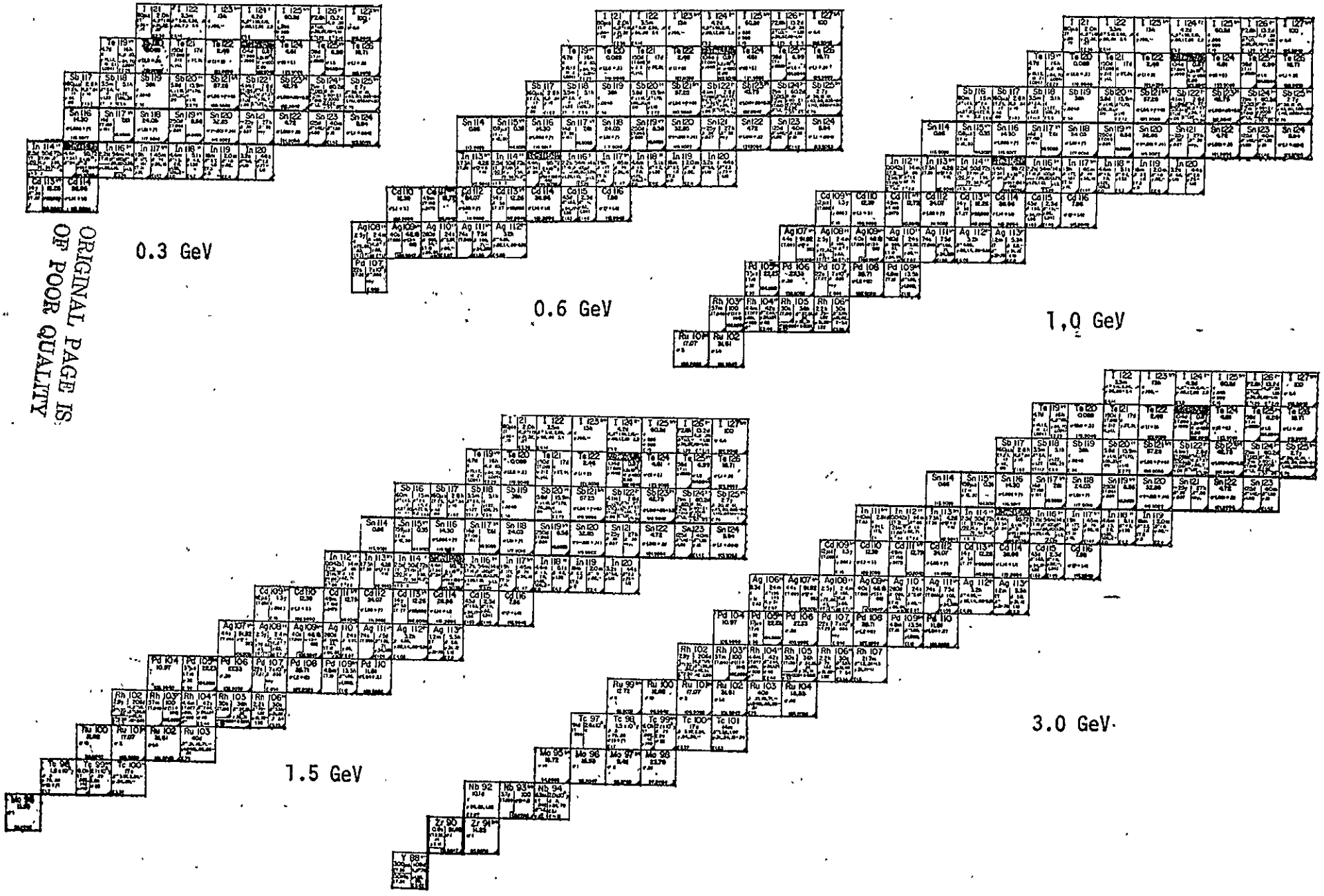

ORIGINAL PAGE IS
OF POOR QUALITY

FIGURE 5. IODINE SPALLATION YIELDS, 0.3 TO 3.0 GeV

ORIGINAL PAGE IS
OF POOR QUALITY

NOTE: SODIUM SPALLATION PRODUCTS WITH $\sigma > 10$ mb; $\sigma_t = 410$ mb

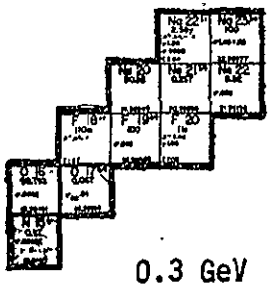

0.3 GeV

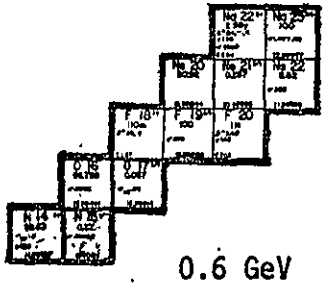

0.6 GeV

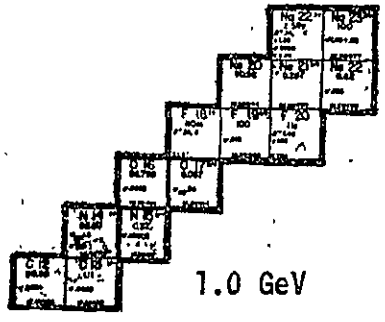

1.0 GeV

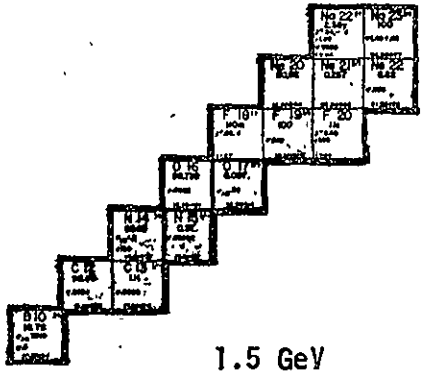

1.5 GeV

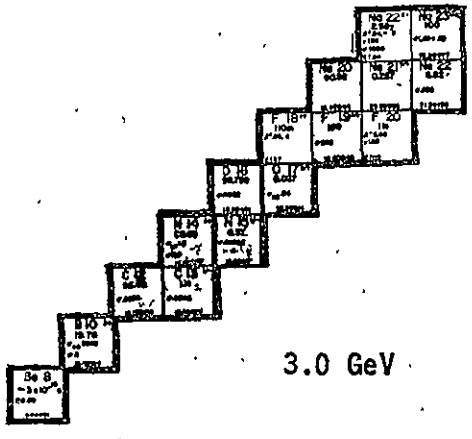

3.0 GeV

FIGURE 6. SODIUM SPALLATION YIELDS, 0.3 TO 3.0 GeV

At an incident energy of 1 GeV, there are 83 spallation nuclides produced in sodium iodide with yield cross sections greater than 10 millibarns (1 millibarn = 10^{-27} cm^2) and 208 nuclides with yield cross sections greater than 1 millibarn. About 70 percent of these nuclides will either be beta-unstable or will have radioactive isomeric states with half-lives greater than 10 microseconds. (It should be noted that the total calculated spallation yield per unit crystal thickness for sodium iodide is only 9 percent less than that of cesium iodide so that the results obtained would apply to either crystal.) At proton energies other than 1 GeV, the cross section distribution of the spallation products changes greatly but the sum of the cross sections remains nearly constant, being approximately equal to the nuclear geometrical cross section of the target nucleus, 1,260 millibarns for iodine and 410 millibarn for sodium.

A rough calculation may be made of the induced counting rate in a spacecraft-borne sodium iodide detector. The rate of detected counts per unit of isotropic detector area, F_c, is given by

$$F_c = f_i f_r f_t m_c F_p \qquad (1)$$

where

F_p - isotropic flux of particles capable of inducing radioactivity

f_i - fraction of F_p which undergoes nuclear interactions within the detector

f_r - fraction of spallation products which are radioactive

f_t - fraction of decays occurring within an allowable observation time

m_c - average number of counts observed within the detector for each radioactive nucleus produced.

Each term will now be considered in more detail.

The term f_i in Equation 1 may be calculated for thin targets composed of j different nuclear species from the formula

$$f_i = \sum_j \frac{N_o \sigma_j X_j}{A_j}$$

where

N_o - Avagadro's number

σ_j - cross section for a cosmic-ray spallation interaction with a target nucleus of atomic weight, A_j

X_j - mass thickness contribution of the target material, j.

Assuming σ_j to be equal to the nuclear geometrical cross section and a typical detector thickness is $X_{NaI} = 25$ gm-cm^{-2}, then $f_i = 0.17$. This is sufficiently smaller than unity so that the thin target approximation is valid and indicates that cosmic-ray secondaries produced within the detector will have a minimal effect on the total spallation production.

The terms f_r, f_t, and m_c were derived from the nuclear decay schemes of over 100 spallation products, weighted according to their production cross section, as derived from the Rudstam formulae. It was found that the values were rather insensitive to the incident proton energy and that they are mainly determined by the nuclear energy level spacing of nuclei with mass numbers near that of the target nucleus. In determining f_t, it was assumed that only those isotopes with half-lives in the range from 10 microseconds to 50 days would contribute to the observed counting rate. The values adopted are $f_r = 0.7$, $f_t = 0.8$, and $m_c = 1.6$. The reason that m_c is greater than unity is, of course, because daughter nuclei of many radioactive transitions are also radioactive. The relatively large value of f_t results from the fact

that the half-lives of most radioactive spallation products are in the minutes-to-days range.

The half-life distribution of radioactive spallation products induced in an iodine target from 1 GeV protons is shown in Figure 7. In this figure, the sum of the cross sections of products within each logarithmic-spaced half-life interval is plotted as a function of the product half-life.

Using the above values for the terms in Equation 1, the calculated counting rate within a 25 gm-cm^{-2} detector (over all detected energies) relative to the inducing particle flux is

$$\frac{F_c}{F_p} = 0.15 \text{ count per incident proton.}$$

This result includes only the effects of the residual target nuclei (spallation products) and not the smaller fragments which are ejected from the target nuclei. With the exception of Be^7, which has a production cross section of approximately 10 millibarns at high energies all of the more abundant fragments that are produced are either very short-lived ($\tau_{\frac{1}{2}} \lesssim 10$ microseconds) or stable and thus do not contribute to the counting rate.

The spectral distribution of the induced counting rate is not easily deduced from the nuclear decay schemes. However, it is noted that the spectrum of gamma rays from a large number of mixed fission products has an exponential form with an e-folding energy of 0.9 MeV (Ref. 9). The average atomic weight of these products is close to that of iodine, and, thus, they have similar nuclear energy level spacings. For the purpose of the present calculations, we will adopt a spectral distribution of the form

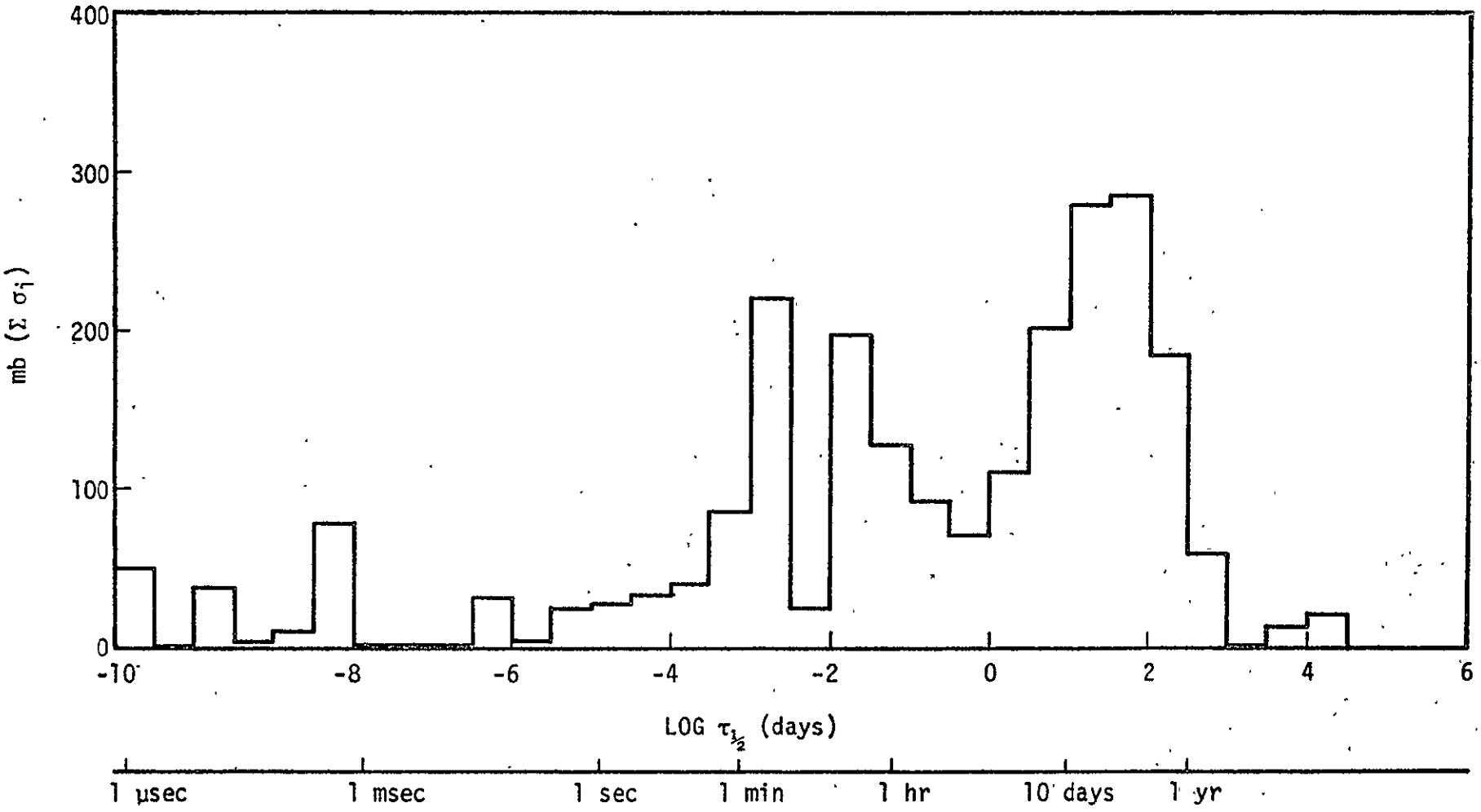

FIGURE 7. HALF-LIFE DISTRIBUTION OF IODINE SPALLATION PRODUCTS

$$\frac{dF_c}{F_p\, dE} = \frac{F_c}{F_p\, E_e} \exp\left(-\frac{E}{E_e}\right) \text{ counts} \cdot \text{MeV}^{-1} \cdot \text{per incident particle}$$

$$E_e = 0.9 \text{ MeV} \quad .$$

The rather coarse assumption of a purely exponential energy-loss spectrum may introduce errors of up to a factor of two at any specific energy from 50 keV to 6 MeV, but the integrated counts in the spectrum are probably accurate to ±20 percent. Indeed, spectral features resulting from electron capture decays of the more abundant radioactive products will certainly be present in the energy-loss spectrum. It should be noted that the observed energy loss will include the K shell binding energy of the parent isotope (33.2 keV for iodine). Listed in Table 1 are the expected spectral lines resulting from electron capture and internal transitions.

TABLE 1. SPECTRAL LINES FROM IODINE SPALLATION PRODUCTS

ISOTOPE	DECAY*	$\tau_{1/2}$	ENERGY (MeV)
I^{126}	EC	13 d	0.667 + 0.033
I^{126}	EC	13 d	1.420 + 0.033
I^{125}	EC	60 d	0.035 + 0.033
I^{124}	EC	4.2 d	0.603 + 0.033
I^{124}	EC	4.2 d	2.295 + 0.033
I^{124}	EC	4.2 d	1.962 + 0.033
I^{123}	EC	13.3 h	0.159 + 0.033
I^{121}	EC	2.1 h	0.212 + 0.033
Te^{125m}	IT	58 d	0.145
Te^{123m}	IT	117 d	0.247
Te^{121m}	IT	154 d	0.293
Te^{121}	EC	17 d	0.573 + 0.032
Sb^{122m}	IT	4.2 m	0.026
Sb^{122m}	IT	530 μsec	0.075
Sb^{122m}	IT	1.8 μsec	0.061

*EC = ELECTRON CAPTURE

IT = INTERNAL TRANSITION

EXPERIMENT

In an effort to directly measure the radioactivity induced in a scintillation detector, an accelerator experiment was performed at the NASA Space Radiation Effects Laboratory, Newport News, Virginia. A sodium iodide detector, 1.7 gm-cm^{-2} thick, was irradiated with a low flux of 600 MeV protons over a 10-second period. The integrated irradiation flux, 7×10^{10} protons in a 5-centimeter-diameter sodium iodide detector, was measured using the known cross section for the I^{127} (p, p 4n) I^{123} reaction as a beam monitor (Ref. 10). The number of I^{123} nuclei produced were derived from the 0.192-MeV line observed in the decay spectrum at a known time after the irradiation. Continuum and background radiation corrections were made to the data in this derivation; however, its accuracy is estimated at only ±30 percent because of the magnitude of the corrections and the uncertainty of the I^{123} cross section.

Counting rate spectra were taken at various times after the irradiation. Several of these spectra are presented in Appendix B. A superposition of five of these spectra is shown in Figure 8. In general, the spectra show exponential continua with several discrete peaks superimposed. Most of the peaks from electron capture and internal transition decays of radioactive isotopes of iodine, tellurium, and antimony in Table 1 could be identified in the spectra. The continuous nature of the spectra arises from the large number of radioactive products involved and the fact that most transitions include a non-discrete beta transition.

Intensity as a function of time after irradiation plots were made for various energy ranges from 0.05 MeV to 3.0 MeV and from 3.5

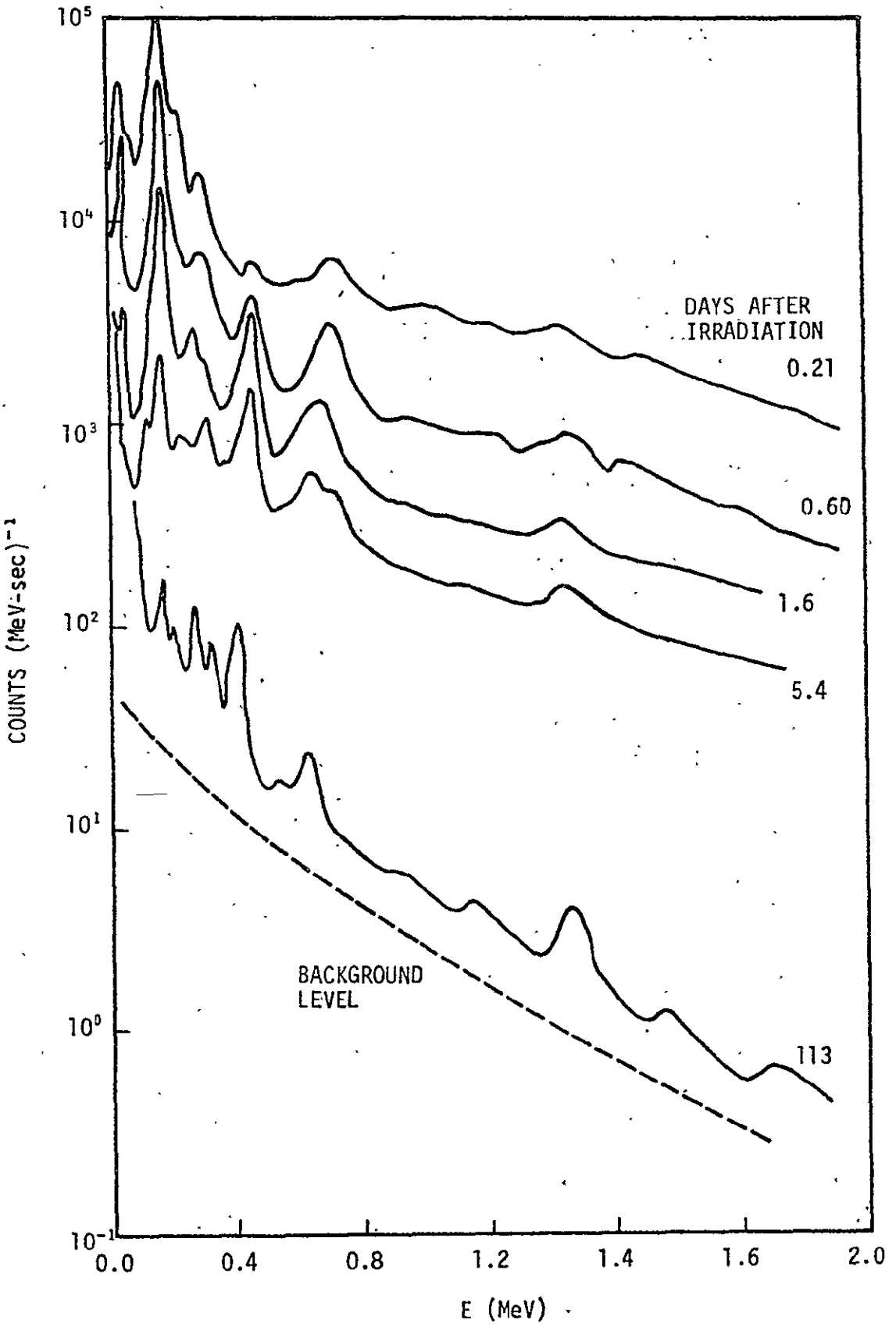

FIGURE 8. ENERGY SPECTRA TAKEN AFTER 600 MeV PROTON IRRADIATION

hours to 50 days after irradiation. These data are presented in Appendix C, and a superposition of the decay curves is shown in Figure 9. Counts prior to 3.5 hours could not be measured accurately because of high counting rates. For each energy interval, the total counts were integrated from 3.5 hours to 50 days following irradiation and then multiplied by a factor 1.8 to account for the undetected counts from 10 microseconds to 3.5 hours after irradiation. The above factor was derived from the half-life distribution of spallation products formed by protons and sodium iodide at 600 MeV, according to the Rudstam formulae. This factor was assumed to be constant over the detected energies. The data were also normalized to a 25 gm-cm^{-2} detector thickness.

Both the calculated cosmic-ray-induced counting rate and the 600-MeV, proton-induced counting rate are plotted in Figure 10. The errors in the measured data, as indicated by the error bars on the lowest energy datum, represent an uncertainty of a factor of 1.5. This uncertainty arises mainly from the determination of the irradiation flux and, thus, represents an absolute error applicable to each measured value. The relative error between the measured data is estimated to be ±20 percent. The error on the calculated data is estimated to be a factor of two, as indicated by the error bars in Figure 10. This factor includes both absolute and relative errors; the relative errors arise from the uncertainty of the spectrum.

The spectrum of the experimental counting rate is slightly softer than the assumed spectral shape; the data above 0.25 MeV can be best fitted by an exponential spectrum with $E_e \approx 0.6$ MeV. However, at each energy, the experimental and calculated induced counting rates agree to within the indicated errors. The energy independence of high-energy spallation radioactivity is supported by the measurements

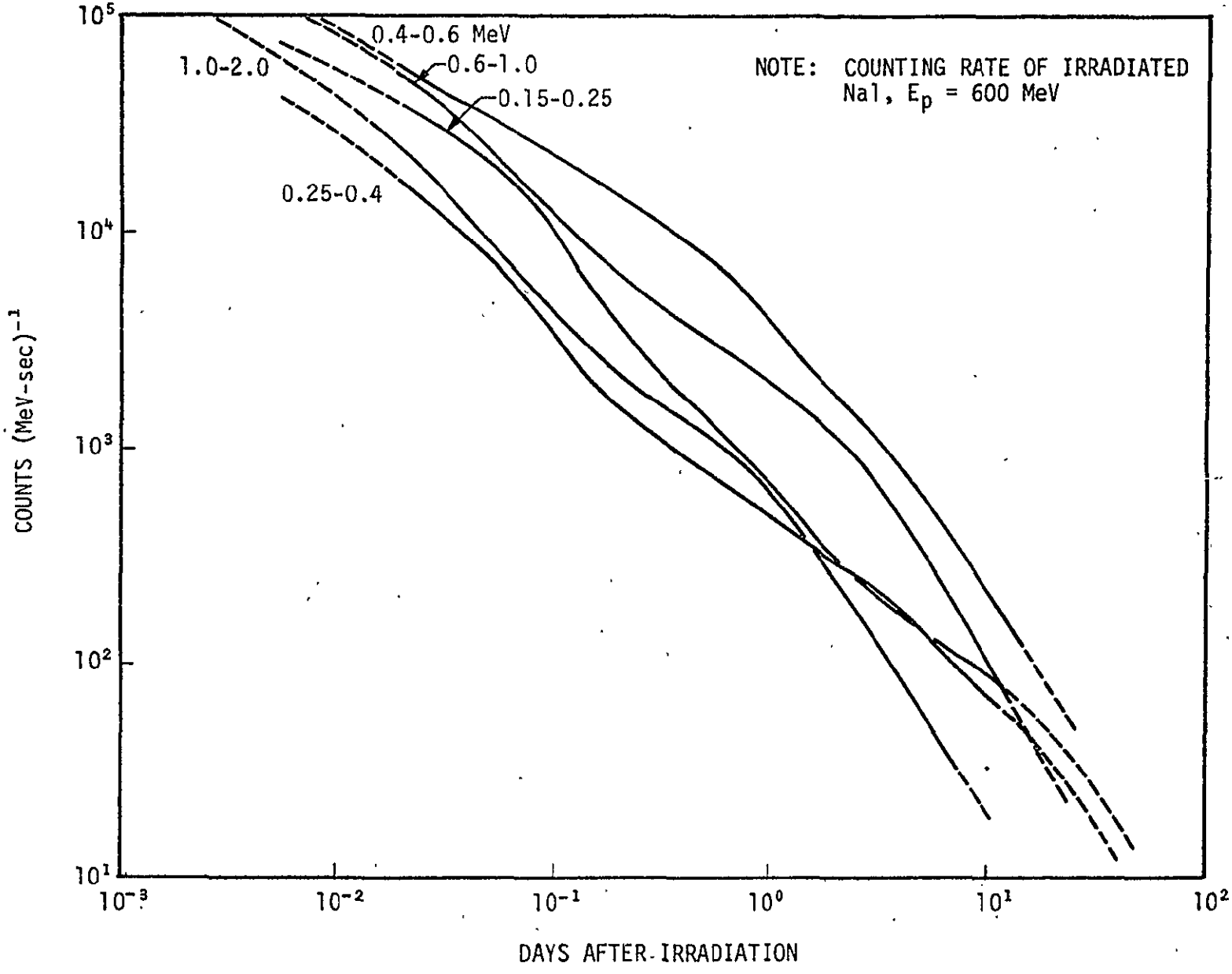

FIGURE 9. INDUCED RADIOACTIVITY DECAY PROFILES

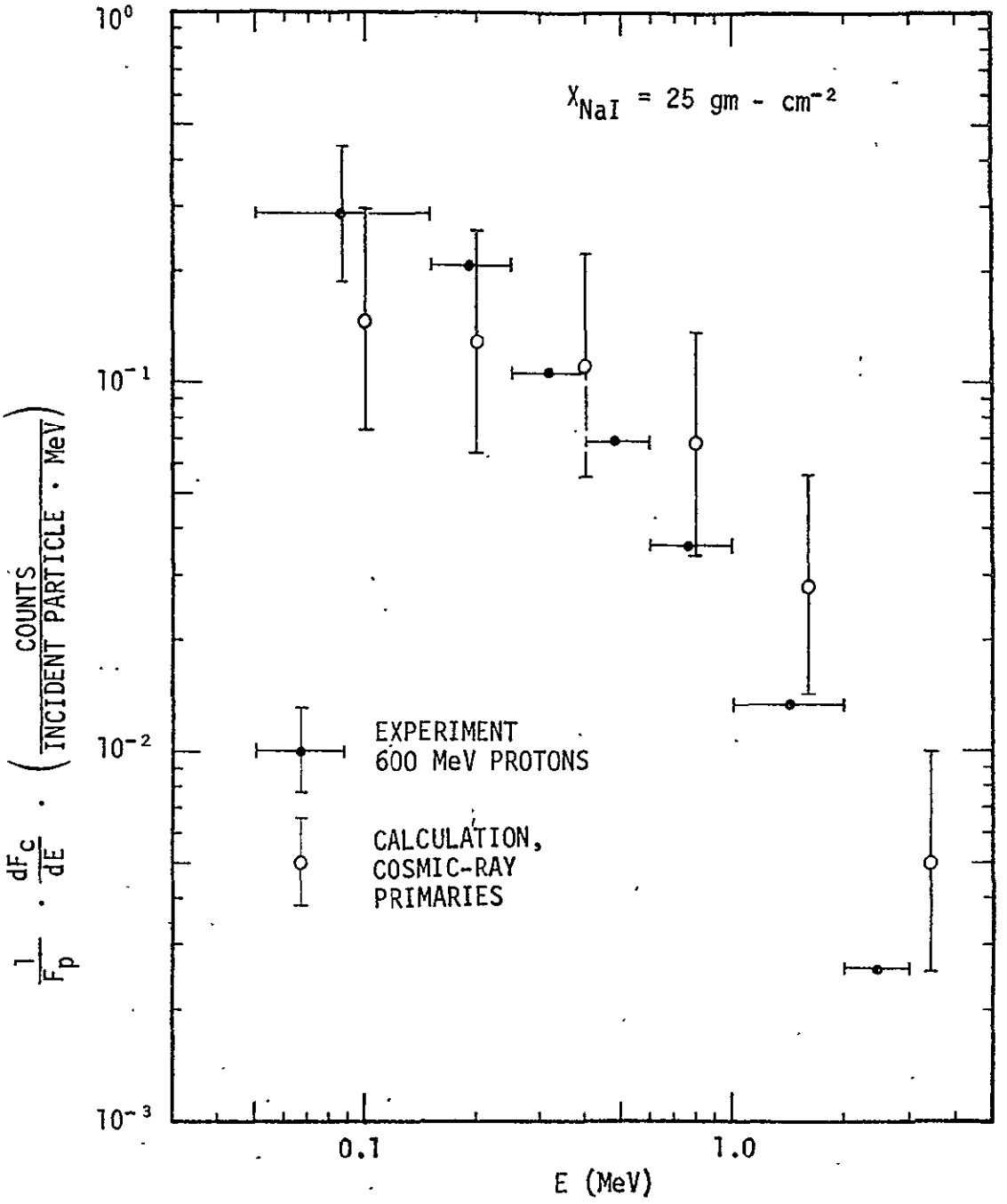

FIGURE 10. CALCULATED AND MEASURED INDUCED RADIOACTIVITY IN A NaI(Tℓ) CRYSTAL

of Barbier (Ref. 11). Those measurements indicate that uranium irradiated by 600 MeV protons produces radioactivity similar to that produced at an irradiation energy of 18 GeV.

SUMMARY AND CONCLUSIONS

The present study indicates that proton-induced radioactivity will be a major source of background radiation for low-level, space-borne detectors in the hard X-ray and gamma-ray regions. Approximately one gamma-ray will be produced after each nuclear interaction. The decay of the induced radioactivity will roughly follow a $1/t$ rate, and the energy spectrum is expected to be exponential with an e-folding energy of ~ 0.9 MeV. Proton irradiation data at 600 MeV are in agreement with the above results.

More precise calculations may be made using experimental cross section data and detailed decay schemes. The actual proton transport within heavy spacecraft will be needed for these calculations, along with the proton dose history. Such calculations are now in progress at the Space Sciences Laboratory/Marshall Space Flight Center.

REFERENCES

1. Stassinopoulos, E. G., "World Maps of Constant B, L and Flux Contours", NASA SP-3054, 1970

2. Lavine, J. P. and J. I. Vette, "Models of the Trapped Radiation Environment, Vol. VI: High Energy Protons", NASA SP-3024, 1970

3. Peterson, L. E., Journal of Geophysical Research, Vol. 70, p. 1762, 1965

4. Golenetskii, S. V., Astrophysical Letters, Vol. 9, p. 69, 1971

5. Dyer, C. S. and G. E. Morfill, Astrophysics and Space Science, Vol. 14, p. 243, 1971

6. Fishman, G. J., The Astrophysical Journal, Vol. 171, p. 163, 1972

7. Rudstam, G., Zeitschrif für Naturforschung, Vol. 21a, p. 1027, 1966

8. Goldman, D. T., "Chart of the Nuclides", 9th Edition, General Electric Company, 1966

9. Goldstein, H., Fundamental Aspects of Reactor Shielding, Reading, Massachusetts: Addison-Wesley Publishing Company, 1959

10. Ladenbauer, J. and L. Winsberg, Physical Review, Vol. 119, p. 1368, 1960

11. Barbier, M., Induced Radioactivity, Amsterdam: North-Holland Publishing Company, 1969

APPENDIX A. NaI SPALLATION YIELDS

PAGE	Z	ELEMENT	ISOTOPES
	SPALLATION YIELDS FOR Na^{23} TARGET		
A-2	11	Na	17-22
A-3	10	Ne	16-22
A-4	9	F	15-21
A-5	8	O	14-20
A-6	7	N	12-19
A-7	6	C	10-18
	SPALLATION YIELDS FOR I^{127} TARGET		
A-8	53	I	116-126
A-9	52	Te	113-126
A-10	51	Sb	111-125
A-11	50	Sn	108-124
A-12	49	In	105-123
A-13	48	Cd	103-122
A-14	47	Ag	100-121
A-15	46	Pd	98-120
A-16	45	Rh	95-119
A-17	44	Ru	92-116
A-18	43	Tc	90-114
A-19	42	Mo	87-111

ORIGINAL PAGE IS
OF POOR QUALITY

A(TARGET) = 23.

Na

Z = 11

E(MEV) =	100.	300.	600.	1000.	3000.
A	CROSS SECTION IN MILLIBARNS				
13	0.0	0.0	0.0	0.0	0.0
14	0.0	0.0	0.0	0.0	0.0
15	0.0	0.0	0.0	0.0	0.0
16	0.0	0.0	0.0	0.0	0.0
17	0.0	0.0	0.0	0.0	0.0
18	0.0	0.0	0.0	0.0	0.0
19	0.0	0.0	0.0	0.0	0.0
20	1.3	0.6	0.5	0.4	0.2
21	18.5	6.1	4.7	3.8	2.4
22	145.2	35.9	25.3	19.4	11.6

ORIGINAL PAGE IS
OF POOR QUALITY

A(TARGET) = 23.

Ne

Z = 10

E(MEV) =	100.	300.	600.	1000.	3000.
A	CROSS SECTION IN MILLIBARNS				
11	0.0	0.0	0.0	0.0	0.0
12	0.0	0.0	0.0	0.0	0.0
13	0.0	0.0	0.0	0.0	0.0
14	0.0	0.0	0.0	0.0	0.0
15	0.0	0.0	0.0	0.0	0.0
16	0.0	0.0	0.0	0.0	0.0
17	0.0	0.0	0.0	0.0	0.0
18	0.4	0.3	0.3	0.3	0.2
19	5.7	3.9	3.7	3.3	2.3
20	54.9	24.1	20.7	17.4	11.7
21	198.0	65.3	50.7	40.7	25.9
22	148.7	36.7	25.9	19.8	11.9

A(TARGET) = 23.

F

Z = 9

E(MEV) =	100.	300.	600.	1000.	3000.
A	CROSS SECTION IN MILLIBARNS				
9	0.0	0.0	0.0	0.0	0.0
10	0.0	0.0	0.0	0.0	0.0
11	0.0	0.0	0.0	0.0	0.0
12	0.0	0.0	0.0	0.0	0.0
13	0.0	0.0	0.0	0.0	0.0
14	0.0	0.0	0.0	0.0	0.0
15	0.0	0.0	0.0	0.0	0.0
16	0.1	0.2	0.2	0.2	0.2
17	2.4	2.5	2.9	2.8	2.2
18	20.6	16.1	16.7	15.4	11.6
19	63.1	37.0	34.9	30.8	21.9
20	40.0	17.6	15.0	12.6	8.5
21	15.1	4.9	3.8	3.1	1.9

A(TARGET) = 23.

0

Z = 8

E(MEV) =	100.	300.	600.	1000.	3000.
A	CROSS SECTION IN MILLIBARNS				
7	0.0	0.0	0.0	0.0	0.0
8	0.0	0.0	0.0	0.0	0.0
9	0.0	0.0	0.0	0.0	0.0
10	0.0	0.0	0.0	0.0	0.0
11	0.0	0.0	0.0	0.0	0.0
12	0.0	0.0	0.0	0.0	0.0
13	0.0	0.0	0.0	0.0	0.0
14	0.0	0.1	0.1	0.1	0.1
15	0.8	1.5	2.2	2.3	2.1
16	7.6	10.7	13.4	13.6	11.5
17	19.5	20.4	23.3	22.5	18.0
18	10.4	8.1	8.4	7.8	5.8
19	3.3	1.9	1.8	1.6	1.1
20	0.8	0.3	0.3	0.2	0.1

A(TARGET) = 23.

N

Z = 7

E(MEV) =	100.	300.	600.	1000.	3000.
A	CROSS SECTION IN MILLIBARNS				
5	0.0	0.0	0.0	0.0	0.0
6	0.0	0.0	0.0	0.0	0.0
7	0.0	0.0	0.0	0.0	0.0
8	0.0	0.0	0.0	0.0	0.0
9	0.0	0.0	0.0	0.0	0.0
10	0.0	0.0	0.0	0.0	0.0
11	0.0	0.0	0.0	0.0	0.0
12	0.0	0.0	0.1	0.1	0.1
13	0.2	0.9	1.5	1.9	1.9
14	2.8	7.0	10.7	11.9	11.3
15	5.8	10.9	15.1	16.1	14.3
16	2.6	3.6	4.5	4.6	3.9
17	0.7	0.7	0.8	0.8	0.6
18	0.1	0.1	0.1	0.1	0.0
19	0.0	0.0	0.0	0.0	0.0

ORIGINAL PAGE IS
OF POOR QUALITY

A(TARGET) = 23.

C

Z = 6

E(MEV) =	100.	300.	600.	1000.	3000.
A	CROSS SECTION IN MILLIBARNS				
3	0.0	0.0	0.0	0.0	0.0
4	0.0	0.0	0.0	0.0	0.0
5	0.0	0.0	0.0	0.0	0.0
6	0.0	0.0	0.0	0.0	0.0
7	0.0	0.0	0.0	0.0	0.0
8	0.0	0.0	0.0	0.0	0.0
9	0.0	0.0	0.0	0.0	0.0
10	0.0	0.0	0.0	0.0	0.0
11	0.0	0.5	1.1	1.5	1.6
12	1.0	4.6	8.5	10.4	11.0
13	1.7	5.6	9.5	11.1	11.1
14	0.6	1.5	2.3	2.5	2.4
15	0.1	0.2	0.3	0.3	0.3
16	0.0	0.0	0.0	0.0	0.0
17	0.0	0.0	0.0	0.0	0.0
18	0.0	0.0	0.0	0.0	0.0

A(TARGET) = 127.

I

Z = 53

E(MEV) =	100.	300.	600.	1000.	3000.
A	CROSS SECTION IN MILLIBARNS				
116	0.0	0.0	0.1	0.1	0.1
117	0.0	0.2	0.4	0.5	0.4
118	0.3	0.7	1.1	1.2	1.0
119	1.1	2.0	2.7	2.8	2.2
120	3.7	5.1	6.2	6.1	4.5
121	11.8	12.0	13.4	12.6	8.8
122	35.3	26.9	27.2	24.3	16.1
123	98.5	56.4	51.7	44.1	27.6
124	256.3	110.1	91.7	74.6	44.2
125	616.6	198.6	150.2	116.7	65.2
126	1344.3	324.7	222.9	165.3	87.3

A(TARGET) = 127.

Te

Z = 52

E(MEV) =	100.	300.	600.	1000.	3000.
A	CROSS SECTION IN MILLIBARNS				
113	0.0	0.0	0.0	0.1	0.1
114	0.0	0.1	0.2	0.2	0.3
115	0.0	0.3	0.6	0.7	0.7
116	0.1	0.8	1.4	1.7	1.6
117	0.6	2.1	3.4	3.9	3.4
118	2.1	5.1	7.6	8.2	6.8
119	6.5	11.8	15.9	16.3	12.8
120	18.5	25.1	30.8	30.2	22.4
121	49.0	49.9	55.5	52.0	36.5
122	119.4	91.3	92.2	82.4	54.6
123	263.2	150.8	138.4	118.0	73.9
124	468.7	201.4	167.7	136.5	80.8
125	649.8	209.3	158.3	123.0	68.8
126	817.5	197.4	135.6	100.5	53.1

A(TARGET) = 127.

Sb

Z = 51

E(MEV) =	100.	300.	600.	1000.	3000.
A	CROSS SECTION IN MILLIBARNS				
111	0.0	0.0	0.1	0.1	0.2
112	0.0	0.1	0.3	0.4	0.5
113	0.0	0.3	0.7	1.0	1.1
114	0.1	0.8	1.8	2.4	2.5
115	0.3	2.1	4.2	5.2	5.2
116	1.1	5.0	9.-	10.7	9.9
117	3.4	10.9	17.9	20.2	17.8
118	9.1	22.2	33.0	35.6	29.6
119	22.8	41.4	55.8	57.4	45.1
120	51.1	69.5	85.1	83.5	62.0
121	92.8	94.6	105.3	98.6	69.2
122	128.5	98.2	99.2	88.7	58.8
123	160.6	92.0	84.4	72.0	45.1
124	186.6	80.1	66.7	54.3	32.1
125	204.7	65.9	49.8	38.7	21.6

A(TARGET) = 127.

Sn

Z = 50

E(MEV) =	100.	300.	600.	1000.	3000.
A	CROSS SECTION IN MILLIBARNS				
108	0.0	0.0	0.0	0.0	0.1
109	0.0	0.0	0.1	0.2	0.3
110	0.0	0.1	0.3	0.6	0.8
111	0.0	0.3	0.9	1.4	1.8
112	0.0	0.8	2.3	3.2	3.8
113	0.2	2.0	5.0	6.8	7.5
114	0.6	4.6	10.2	13.2	13.8
115	1.6	9.7	19.2	23.8	23.5
116	4.2	18.4	33.3	39.4	36.7
117	9.8	31.6	51.8	58.5	51.5
118	18.4	44.7	66.4	71.6	59.5
119	25.7	46.6	63.0	64.8	50.9
120	32.0	43.5	53.4	52.4	38.9
121	36.9	37.6	41.9	39.2	27.5
122	40.0	30.6	30.9	27.6	18.3
123	41.3	23.6	21.7	18.5	11.6
124	40.8	17.5	14.6	11.8	7.0

A(TARGET) = 127

In

Z = 49

E(MEV) =	100.	300.	600.	1000.	3000.
A	CROSS SECTION IN MILLIBARNS				
105	0.0	0.0	0.0	0.0	0.0
106	0.0	0.0	0.0	0.1	0.2
107	0.0	0.0	0.1	0.3	0.5
108	0.0	0.1	0.4	0.8	1.2
109	0.0	0.3	1.1	1.9	2.7
110	0.0	0.8	2.7	4.2	5.5
111	0.1	1.9	5.6	8.4	10.4
112	0.3	4.1	10.9	15.6	18.3
113	0.7	8.1	19.5	26.5	29.3
114	1.8	14.2	31.2	40.5	42.2
115	3.6	21.1	42.0	52.1	51.3
116	5.2	22.4	40.4	47.8	44.5
117	6.4	20.9	34.3	38.7	34.1
118	7.4	18.0	26.7	28.8	24.0
119	8.0	14.5	19.6	20.1	15.8
120	8.1	11.1	13.6	13.3	9.9
121	7.9	8.1	9.0	8.4	5.9
122	7.4	5.6	5.7	5.1	3.4
123	6.7	3.8	3.5	3.0	1.8

A(TARGET) = 127.

Cd

Z = 48

E(MEV) =	100.	300.	600.	1000.	3000.
A	CROSS SECTION IN MILLIBARNS				
103	0.0	0.0	0.0	0.0	0.1
104	0.0	0.0	0.0	0.1	0.3
105	0.0	0.0	0.2	0.4	0.8
106	0.0	0.1	0.6	1.1	1.8
107	0.0	0.3	1.4	2.5	3.9
108	0.0	0.7	3.0	5.2	7.6
109	0.0	1.7	6.1	10.0	13.8
110	0.1	3.4	11.2	17.5	22.9
111	0.3	6.3	18.4	27.6	34.1
112	0.7	9.9	26.3	37.5	43.8
113	1.0	10.8	26.2	35.7	39.4
114	1.3	10.2	22.3	29.0	30.3
115	1.5	8.7	17.4	21.6	21.3
116	1.6	7.0	12.7	15.0	13.9
117	1.6	5.3	8.7	9.8	8.6
118	1.5	3.8	5.7	6.1	5.1
119	1.4	2.6	3.5	3.6	2.9
120	1.3	1.7	2.1	2.1	1.5
121	1.1	1.1	1.2	1.1	0.8
122	0.9	0.7	0.7	0.6	0.4

A(TARGET) = 127.

Ag

Z = 47

E(MEV) =	100.	300.	600.	1000.	3000.
A	CROSS SECTION IN MILLIBARNS				
100	0.0	0.0	0.0	0.0	0.0
101	0.0	0.0	0.0	0.0	0.2
102	0.0	0.0	0.1	0.2	0.5
103	0.0	0.0	0.2	0.6	1.2
104	0.0	0.1	0.7	1.4	2.6
105	0.0	0.3	1.5	3.1	5.4
106	0.0	0.6	3.3	6.2	10.2
107	0.0	1.4	6.2	11.3	17.5
108	0.0	2.7	10.7	18.4	27.1
109	0.1	4.5	16.0	26.3	36.4
110	0.2	5.3	17.1	26.8	35.1
111	0.2	5.0	14.8	22.1	27.3
112	0.3	4.3	11.5	16.5	19.3
113	0.3	3.4	8.4	11.4	12.6
114	0.3	2.6	5.7	7.4	7.7
115	0.3	1.8	3.7	4.6	4.5
116	0.2	1.2	2.3	2.7	2.5
117	0.2	0.8	1.3	1.5	1.3
118	0.2	0.5	0.7	0.8	0.7
119	0.1	0.3	0.4	0.4	0.3
120	0.1	0.1	0.2	0.2	0.1
121	0.1	0.1	0.1	0.1	0.0

ORIGINAL PAGE IS
OF POOR QUALITY

A(TARGET) = 127.

Pd

Z = 46

A	E(MEV) = 100.	300.	600.	1000.	3000.
	CROSS SECTION IN MILLIBARNS				
98	0.0	0.0	0.0	0.0	0.1
99	0.0	0.0	0.0	0.1	0.3
100	0.0	0.0	0.1	0.3	0.7
101	0.0	0.0	0.3	0.8	1.7
102	0.0	0.1	0.8	1.8	3.7
103	0.0	0.2	1.7	3.7	7.3
104	0.0	0.5	3.4	7.1	13.0
105	0.0	1.1	6.1	12.1	21.0
106	0.0	2.0	9.5	18.0	29.6
107	0.0	2.6	11.2	20.2	31.3
108	0.0	2.5	9.9	17.0	24.9
109	0.0	2.2	7.8	12.8	17.7
110	0.0	1.7	5.6	8.8	11.6
111	0.0	1.3	3.8	5.7	7.1
112	0.0	0.9	2.4	3.5	4.1
113	0.0	0.6	1.5	2.0	2.2
114	0.0	0.4	0.8	1.1	1.2
115	0.0	0.2	0.5	0.6	0.6
116	0.0	0.1	0.2	0.3	0.3
117	0.0	0.0	0.1	0.1	0.1
118	0.0	0.0	0.0	0.0	0.0
119	0.0	0.0	0.0	0.0	0.0
120	0.0	0.0	0.0	0.0	0.0

A(TARGET) = 127.

Rh

Z = 45

E(MEV) = 100. 300. 600. 1000. 3000.

A	CROSS SECTION IN MILLIBARNS				
95	0.0	0.0	0.0	0.0	0.0
96	0.0	0.0	0.0	0.0	0.1
97	0.0	0.0	0.0	0.1	0.4
98	0.0	0.0	0.1	0.4	1.1
99	0.0	0.0	0.3	1.0	2.4
100	0.0	0.1	0.8	2.1	5.0
101	0.0	0.2	1.8	4.3	9.4
102	0.0	0.4	3.3	7.7	15.8
103	0.0	0.8	5.5	12.1	23.5
104	0.0	1.2	7.3	15.1	27.9
105	0.0	1.2	6.7	13.2	23.0
106	0.0	1.1	5.3	10.1	16.6
107	0.0	0.9	3.9	7.0	10.9
108	0.0	0.6	2.6	4.5	6.6
109	0.0	0.4	1.6	2.7	3.8
110	0.0	0.3	1.0	1.6	2.1
111	0.0	0.2	0.5	0.8	1.1
112	0.0	0.1	0.3	0.4	0.5
113	0.0	0.0	0.1	0.2	0.2
114	0.0	0.0	0.0	0.1	0.1
115	0.0	0.0	0.0	0.0	0.0
116	0.0	0.0	0.0	0.0	0.0
117	0.0	0.0	0.0	0.0	0.0
118	0.0	0.0	0.0	0.0	0.0
119	0.0	0.0	0.0	0.0	0.0

A(TARGET) = 127.

Ru

Z = 44

E(MEV) =	100.	300.	600.	1000.	3000.
A	CROSS SECTION IN MILLIBARNS				
92	0.0	0.0	0.0	0.0	0.0
93	0.0	0.0	0.0	0.0	0.0
94	0.0	0.0	0.0	0.0	0.2
95	0.0	0.0	0.0	0.2	0.6
96	0.0	0.0	0.1	0.5	1.5
97	0.0	0.0	0.4	1.2	3.3
98	0.0	0.0	0.9	2.5	6.5
99	0.0	0.1	1.8	4.7	11.6
100	0.0	0.3	3.1	7.9	18.2
101	0.0	0.6	4.6	11.0	24.1
102	0.0	0.6	4.5	10.3	21.3
103	0.0	0.5	3.7	8.0	15.7
104	0.0	0.4	2.7	5.6	10.4
105	0.0	0.3	1.8	3.6	6.4
106	0.0	0.2	1.1	2.2	3.6
107	0.0	0.1	0.7	1.2	2.0
108	0.0	0.1	0.4	0.7	1.0
109	0.0	0.0	0.2	0.3	0.5
110	0.0	0.0	0.1	0.1	0.2
111	0.0	0.0	0.0	0.0	0.1
112	0.0	0.0	0.0	0.0	0.0
113	0.0	0.0	0.0	0.0	0.0
114	0.0	0.0	0.0	0.0	0.0
115	0.0	0.0	0.0	0.0	0.0
116	0.0	0.0	0.0	0.0	0.0

A(TARGET) = 127.

Tc

Z = 43

E(MEV) =	100.	300.	600.	1000.	3000.
A	CROSS SECTION IN MILLIBARNS				
90	0.0	0.0	0.0	0.0	0.0
91	0.0	0.0	0.0	0.0	0.1
92	0.0	0.0	0.0	0.1	0.3
93	0.0	0.0	0.0	0.2	0.9
94	0.0	0.0	0.1	0.6	2.1
95	0.0	0.0	0.4	1.4	4.4
96	0.0	0.0	0.9	2.8	8.2
97	0.0	0.1	1.7	5.0	13.6
98	0.0	0.2	2.7	7.5	19.5
99	0.0	0.3	3.0	8.0	19.7
100	0.0	0.3	2.6	6.5	15.0
101	0.0	0.2	1.9	4.6	10.1
102	0.0	0.1	1.3	3.0	6.2
103	0.0	0.1	0.8	1.8	3.6
104	0.0	0.0	0.5	1.0	1.9
105	0.0	0.0	0.2	0.5	1.0
106	0.0	0.0	0.1	0.3	0.4
107	0.0	0.0	0.0	0.1	0.2
108	0.0	0.0	0.0	0.0	0.1
109	0.0	0.0	0.0	0.0	0.0
110	0.0	0.0	0.0	0.0	0.0
111	0.0	0.0	0.0	0.0	0.0
112	0.0	0.0	0.0	0.0	0.0
113	0.0	0.0	0.0	0.0	0.0
114	0.0	0.0	0.0	0.0	0.0

ORIGINAL PAGE IS
OF POOR QUALITY

A(TARGET) = 127.

Mo

Z = 42

E(MEV) =	100.	300.	600.	1000.	3000.
A	CROSS SECTION IN MILLIBARNS				
87	0.0	0.0	0.0	0.0	0.0
88	0.0	0.0	0.0	0.0	0.0
89	0.0	0.0	0.0	0.0	0.2
90	0.0	0.0	0.0	0.1	0.5
91	0.0	0.0	0.0	0.3	1.2
92	0.0	0.0	0.2	0.7	2.8
93	0.0	0.0	0.4	1.6	5.5
94	0.0	0.0	0.9	3.0	9.8
95	0.0	0.1	1.5	4.9	15.1
96	0.0	0.1	2.0	6.2	18.0
97	0.0	0.1	1.8	5.2	14.4
98	0.0	0.1	1.4	3.8	10.0
99	0.0	0.1	0.9	2.5	6.2
100	0.0	0.0	0.6	1.5	3.6
101	0.0	0.0	0.3	0.9	1.9
102	0.0	0.0	0.2	0.4	1.0
103	0.0	0.0	0.1	0.2	0.4
104	0.0	0.0	0.0	0.1	0.2
105	0.0	0.0	0.0	0.0	0.1
106	0.0	0.0	0.0	0.0	0.0
107	0.0	0.0	0.0	0.0	0.0
108	0.0	0.0	0.0	0.0	0.0
109	0.0	0.0	0.0	0.0	0.0
110	0.0	0.0	0.0	0.0	0.0
111	0.0	0.0	0.0	0.0	0.0

APPENDIX B. 600-MeV PROTON IRRADIATION SPECTRA OF NaI(Tℓ)

Pulse-height spectra were taken using standard commercial laboratory nuclear instrumentation. These spectra were recorded on paper tape and digital magnetic tape for later conversion into punched paper cards. The data on these cards were used in a computer program which normalized the data with respect to energy and accumulation time. The computer-generated histogram plots are reproduced in this appendix. The large peak at the end of several spectra are instrumental artifacts caused by amplifier saturation. Several discrete peaks in each spectrum are identified at the top of each spectrum. Refer to Table 1 for the energy and half-lives of these isotopes.

SPECTRUM	LOCATION*	TIME AFTER IRRADIATION (Days)	ACCUMULATION TIME (sec)
Background	SREL	Pre-Irradiation	2,000
Background	MSFC	Pre-Irradiation	40,000
1	SREL	0.29	100
2	SREL	0.41	100
3	SREL	0.60	100
4	MSFC	1.63	1,000
5	MSFC	2.5	1,000
6	MSFC	5.4	1,000
7	MSFC	7.0	2,000
8	MSFC	15	4,000
9	MSFC	68	80,000
10	MSFC	113	82,000

*SREL = Space Radiation Effects Laboratory, Hampton, Virginia

MSFC = Space Sciences Laboratory, Marshall Space Flight Center

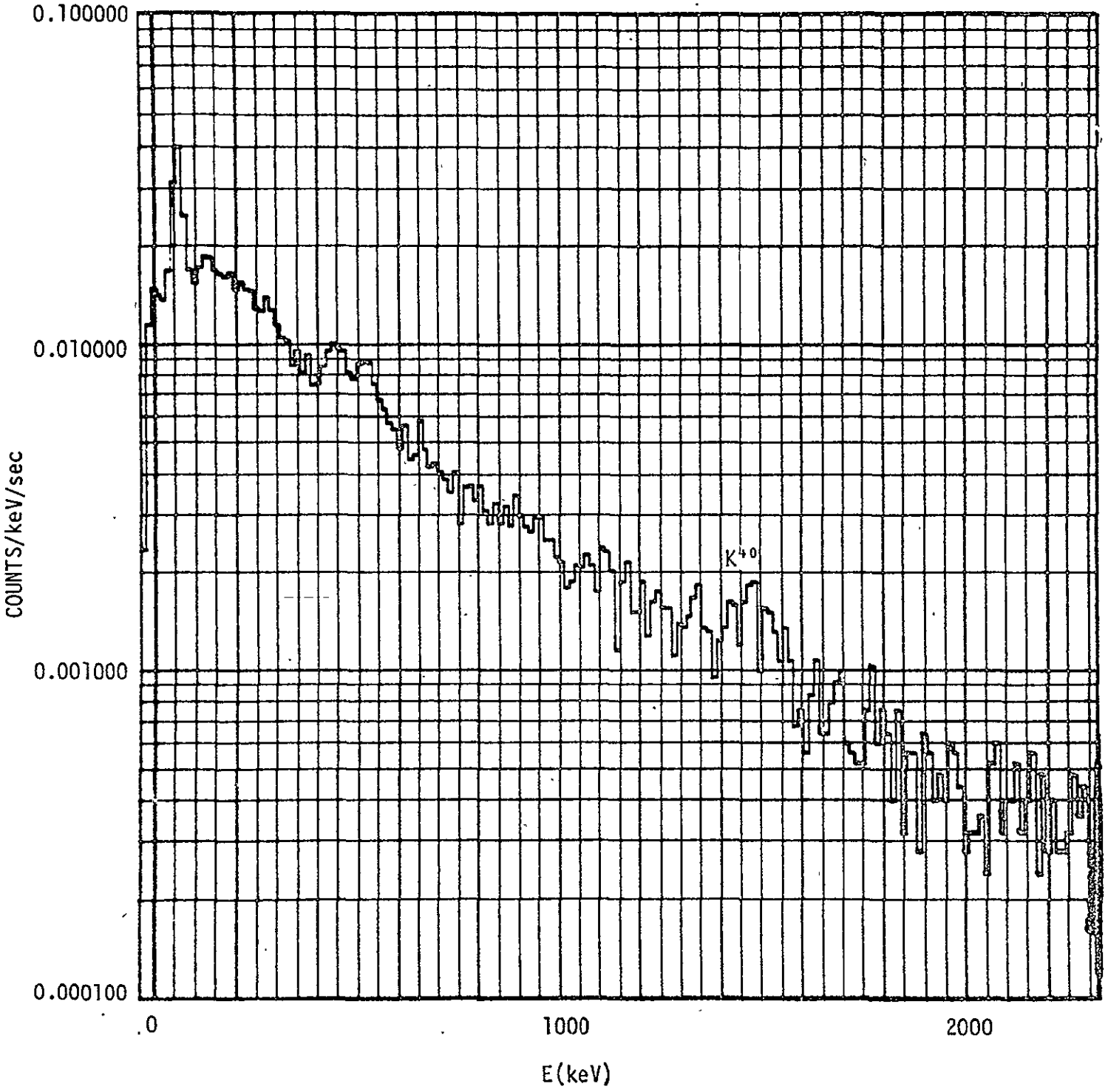

FIGURE B-1. BACKGROUND SPECTRUM, SREL MEASUREMENTS

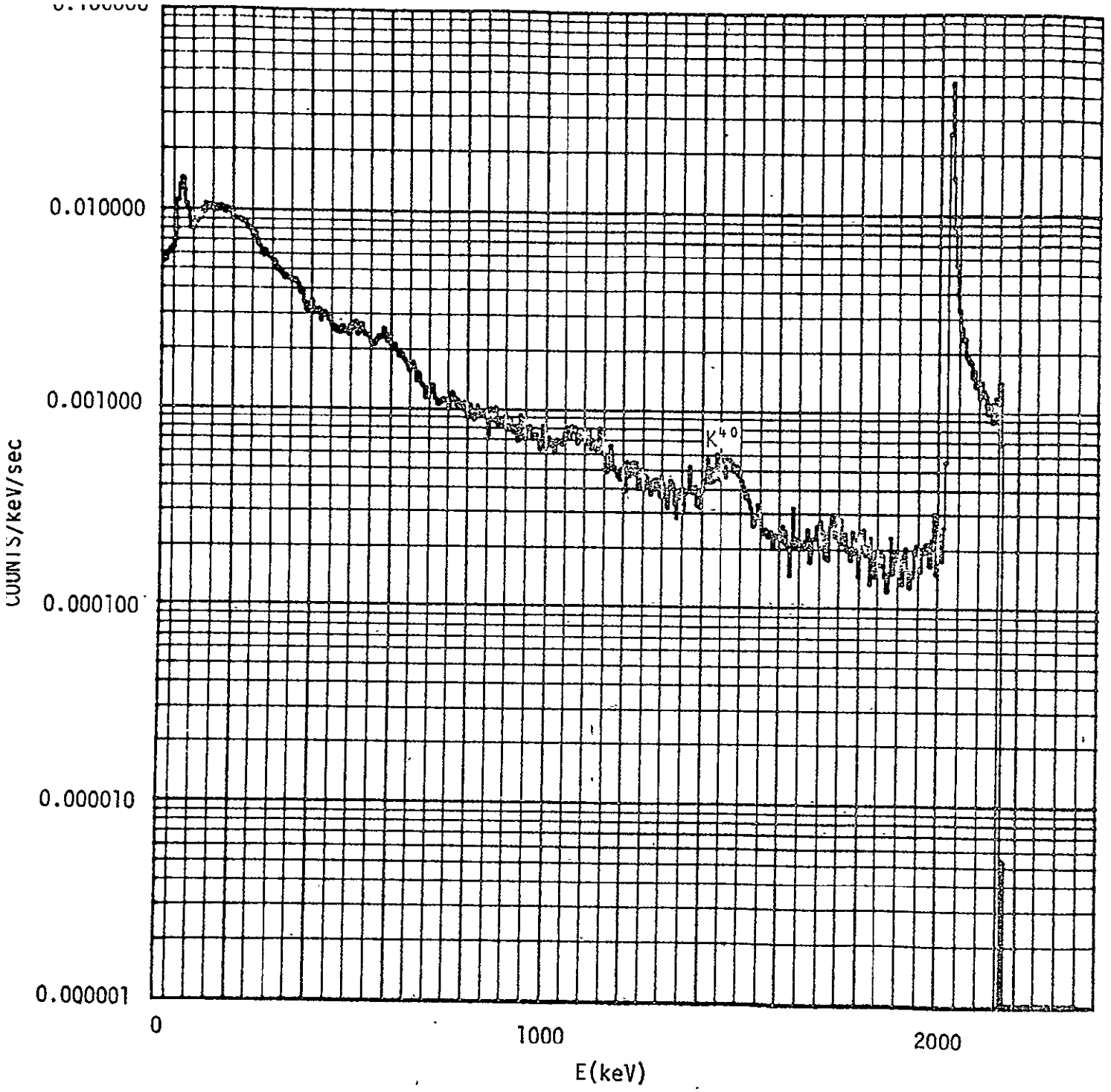

FIGURE B-2. BACKGROUND SPECTRUM, MSFC MEASUREMENTS

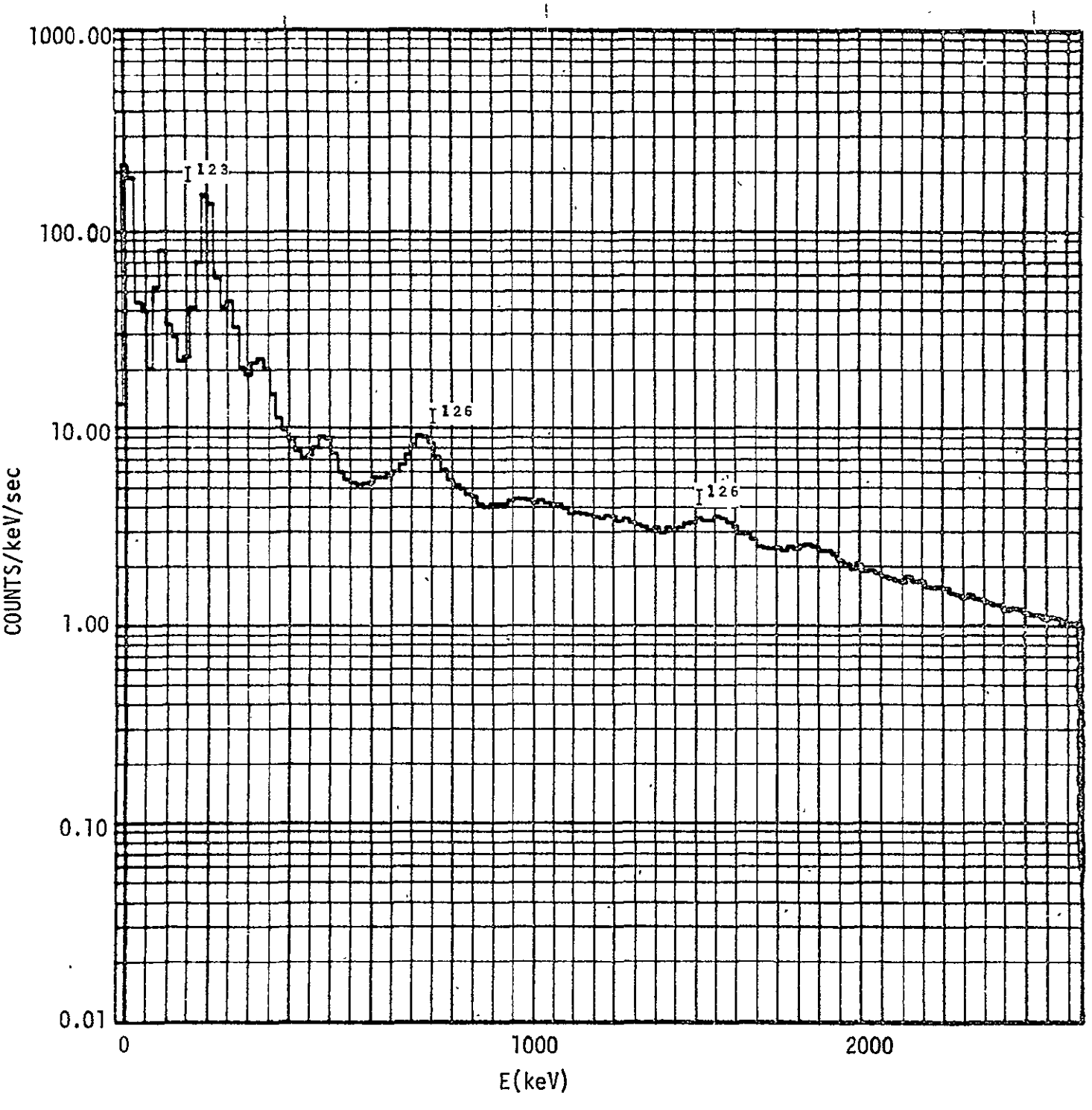

FIGURE B-3. SPECTRUM NUMBER 1

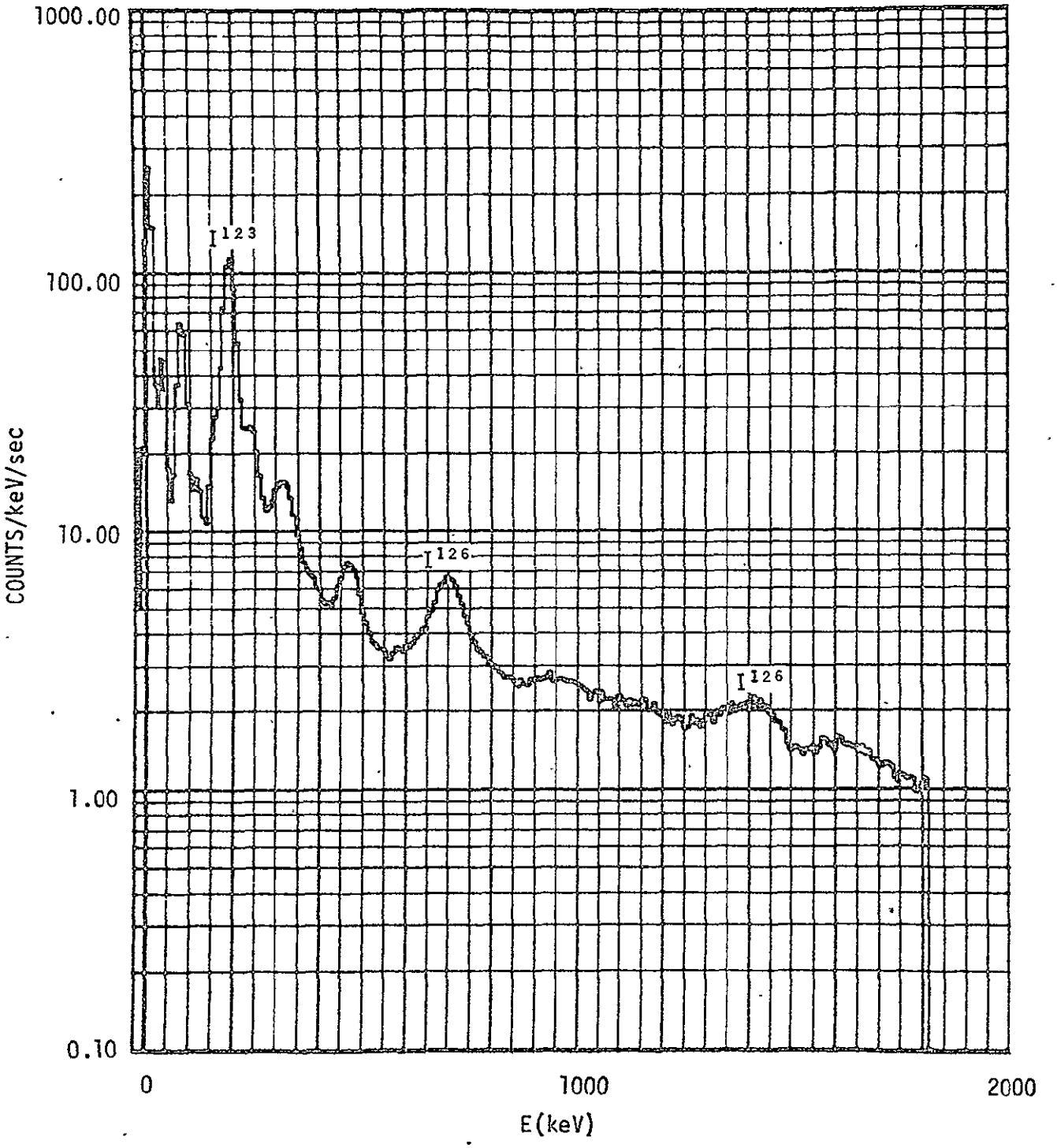

FIGURE B-4. SPECTRUM NUMBER 2

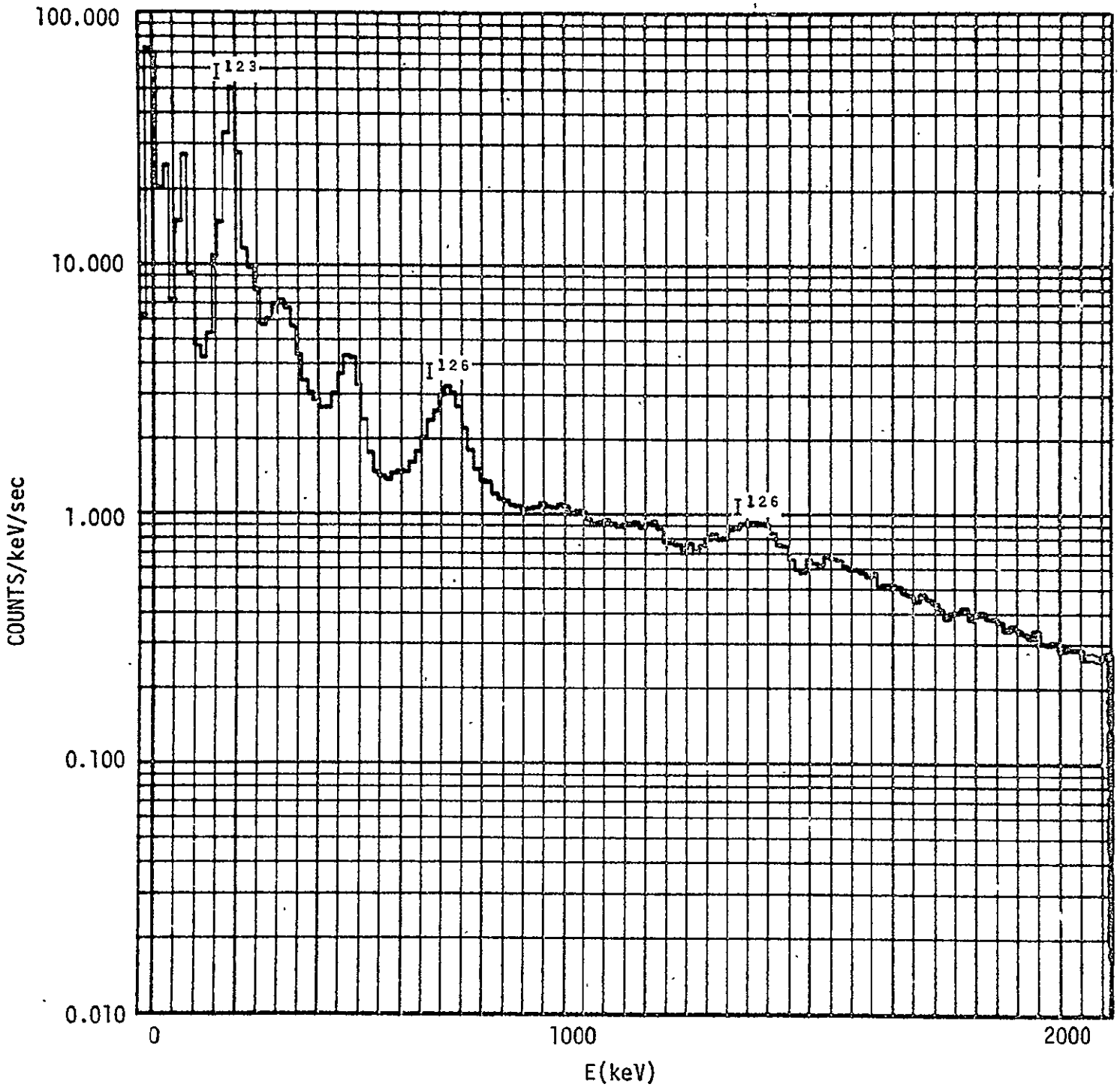

FIGURE B-5. SPECTRUM NUMBER 3

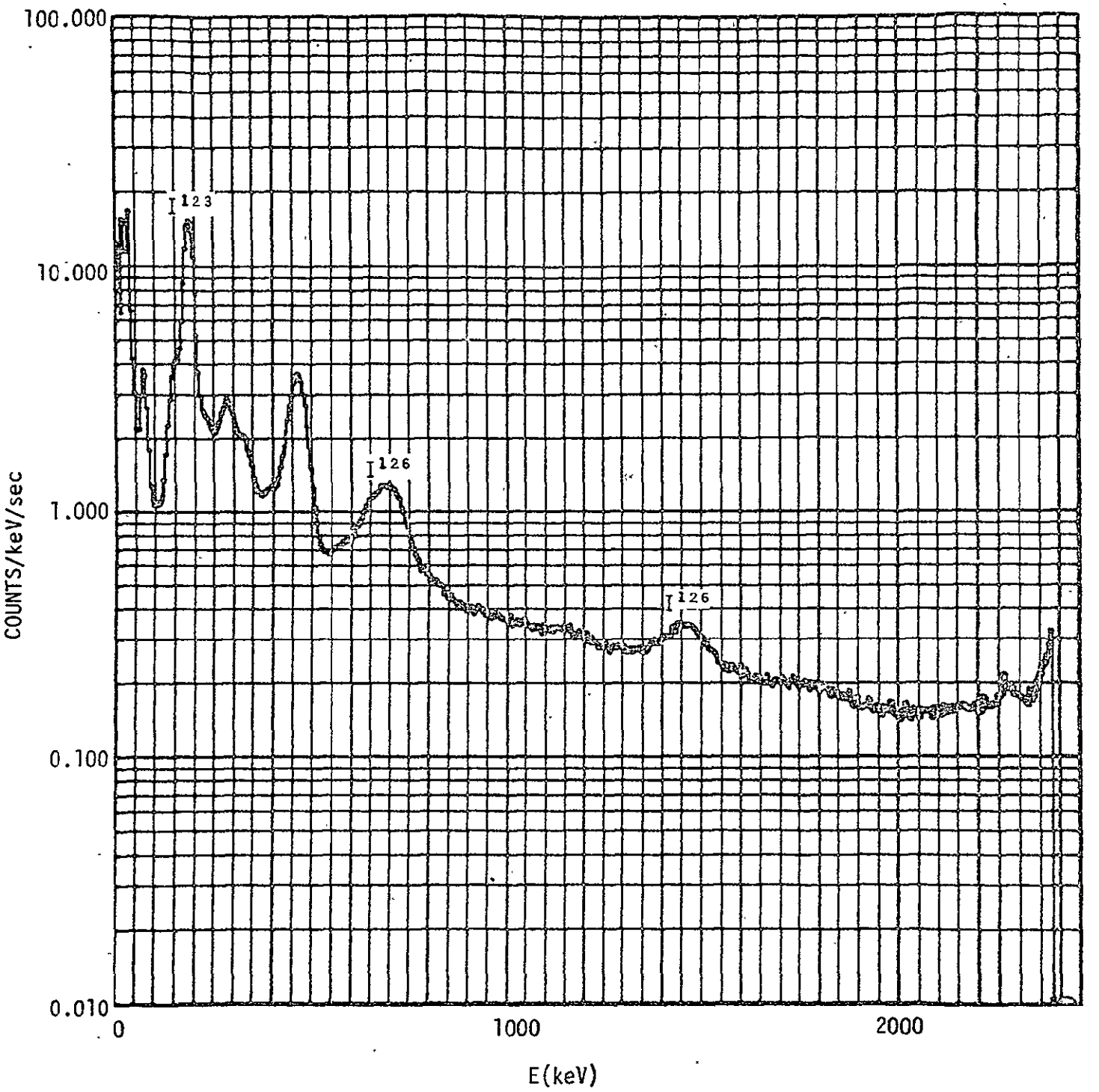

FIGURE B-6. SPECTRUM NUMBER 4

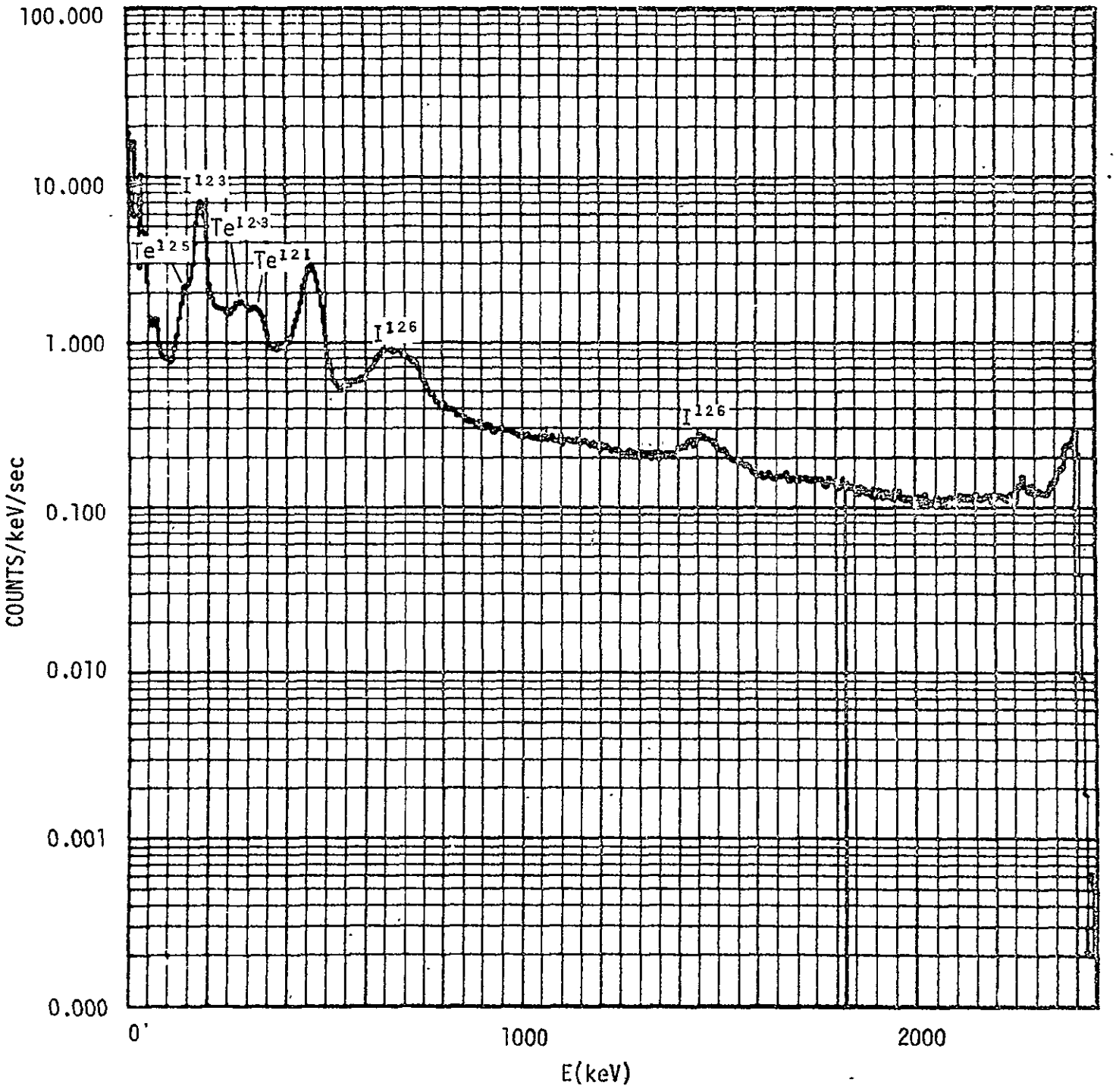

FIGURE B-7. SPECTRUM NUMBER 5

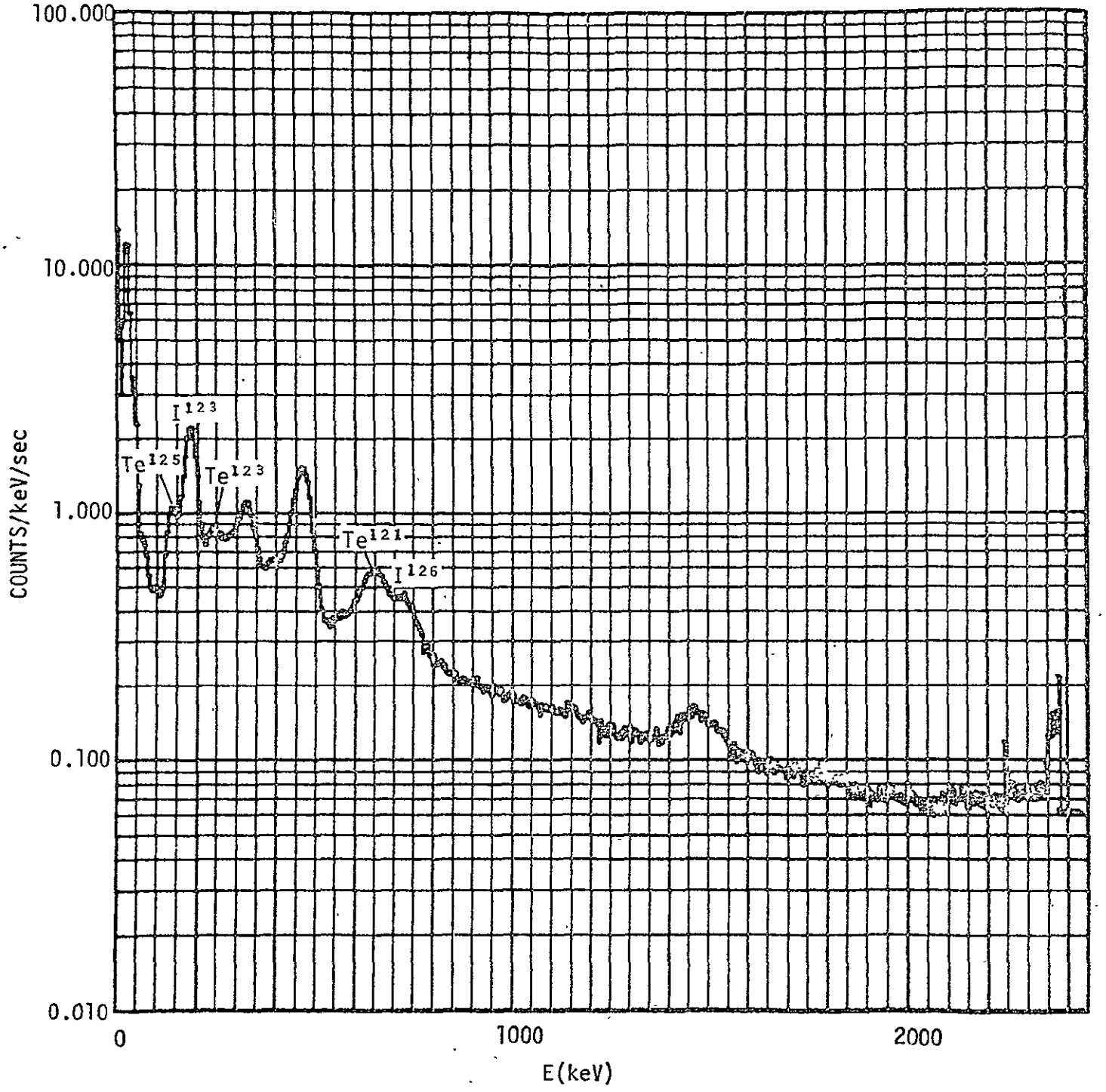

FIGURE B-8. SPECTRUM NUMBER 6

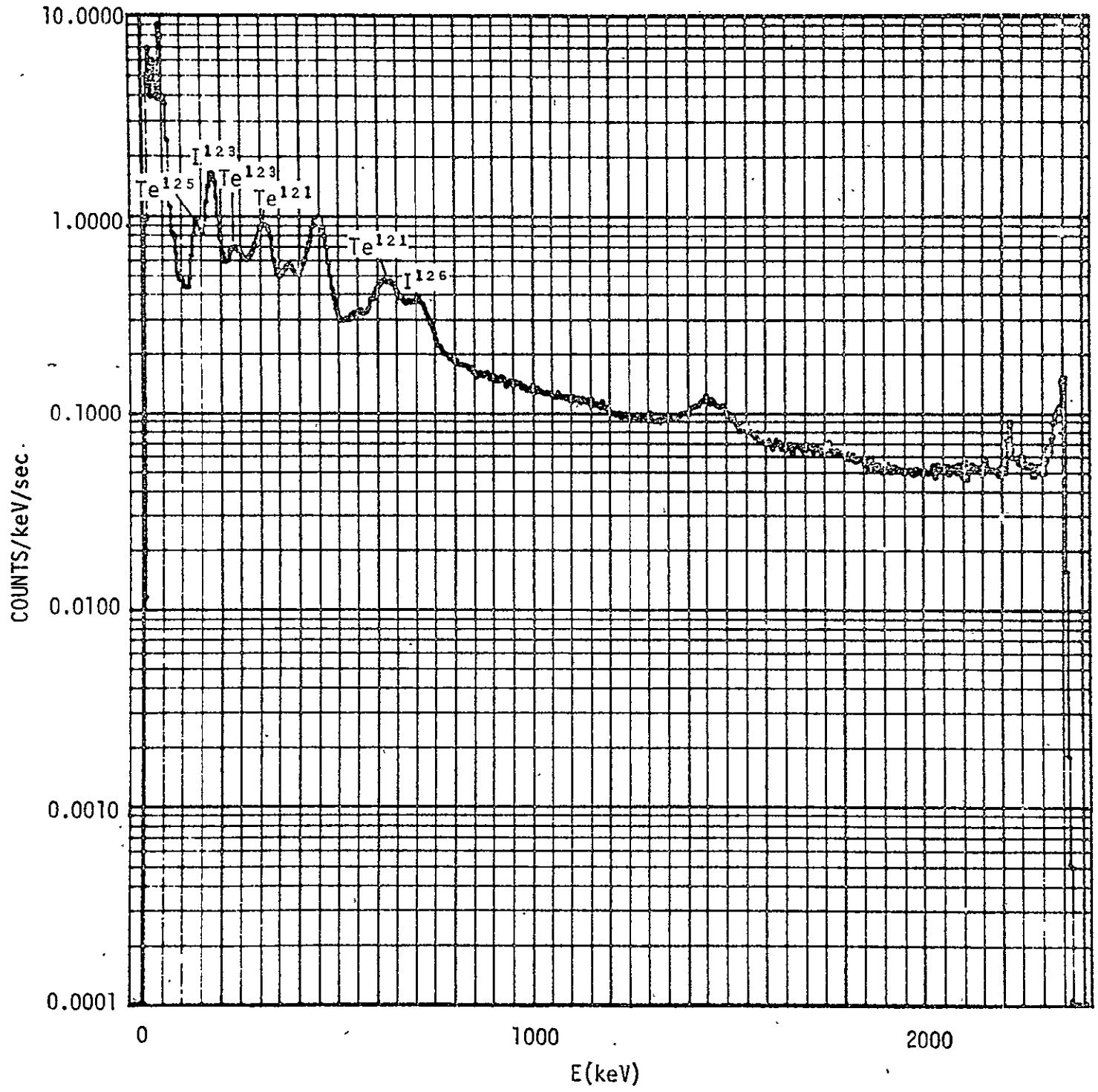

FIGURE B-9. SPECTRUM NUMBER 7

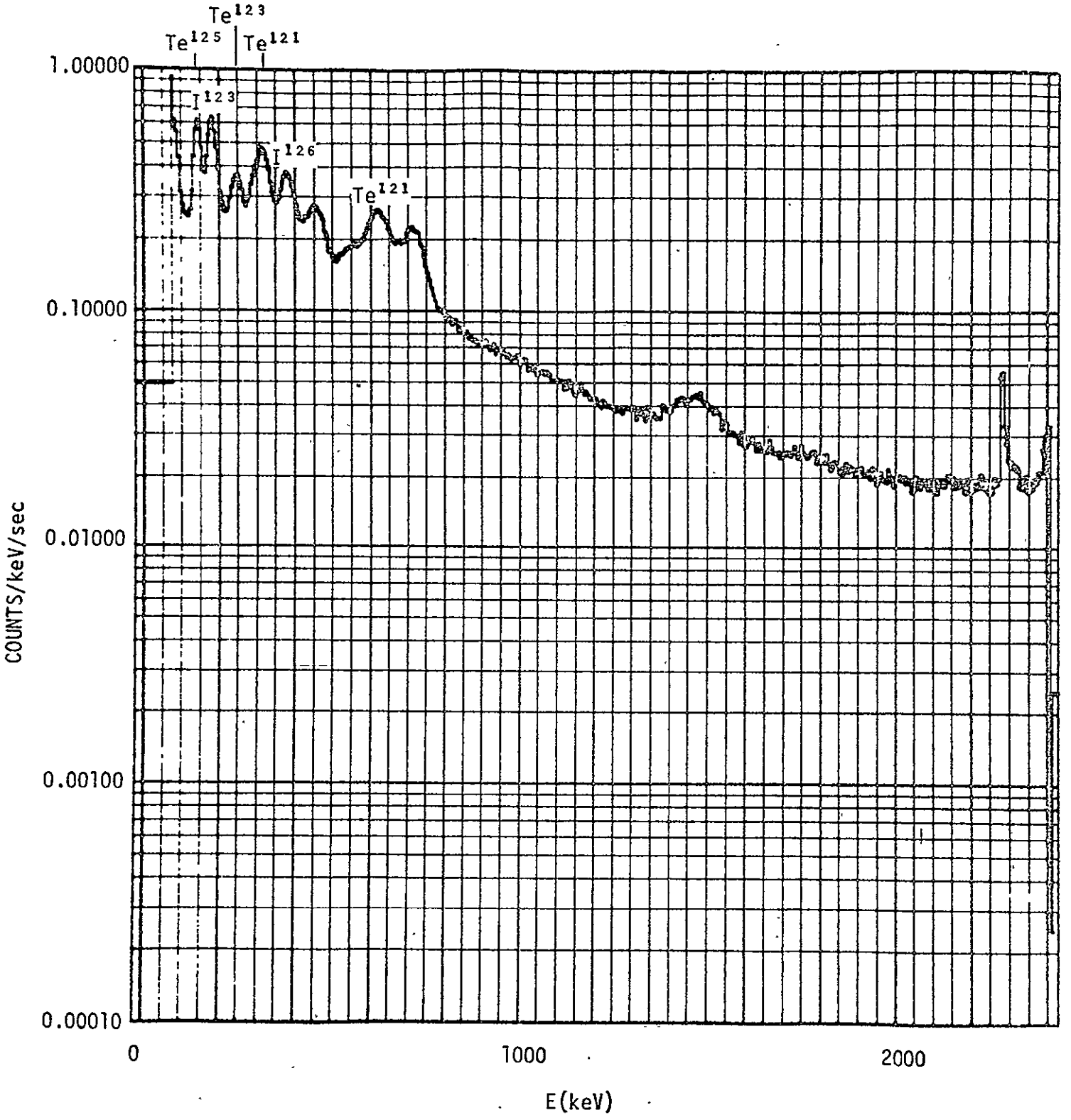

FIGURE B-10. SPECTRUM NUMBER 8

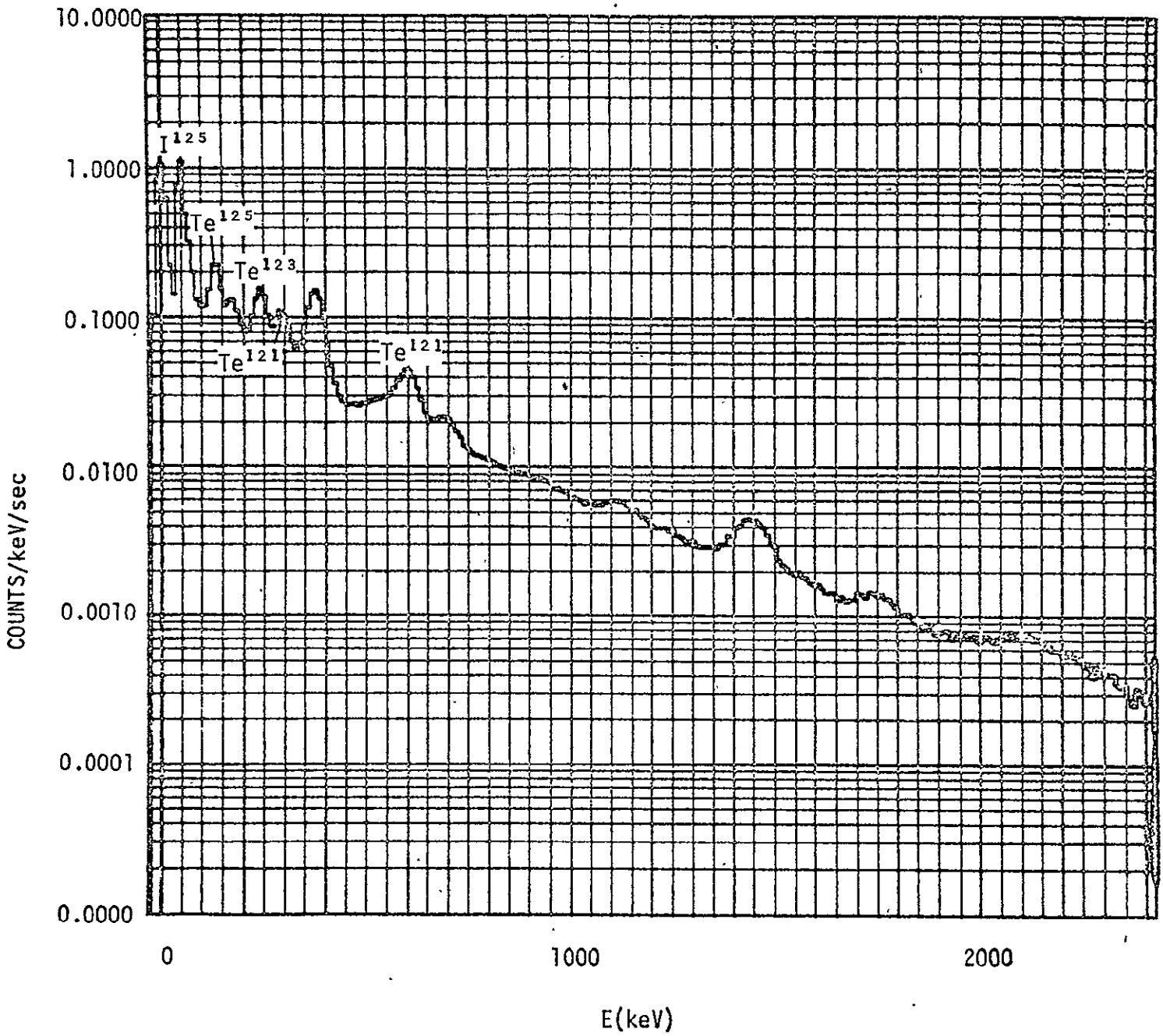

FIGURE B-11. SPECTRUM NUMBER 9

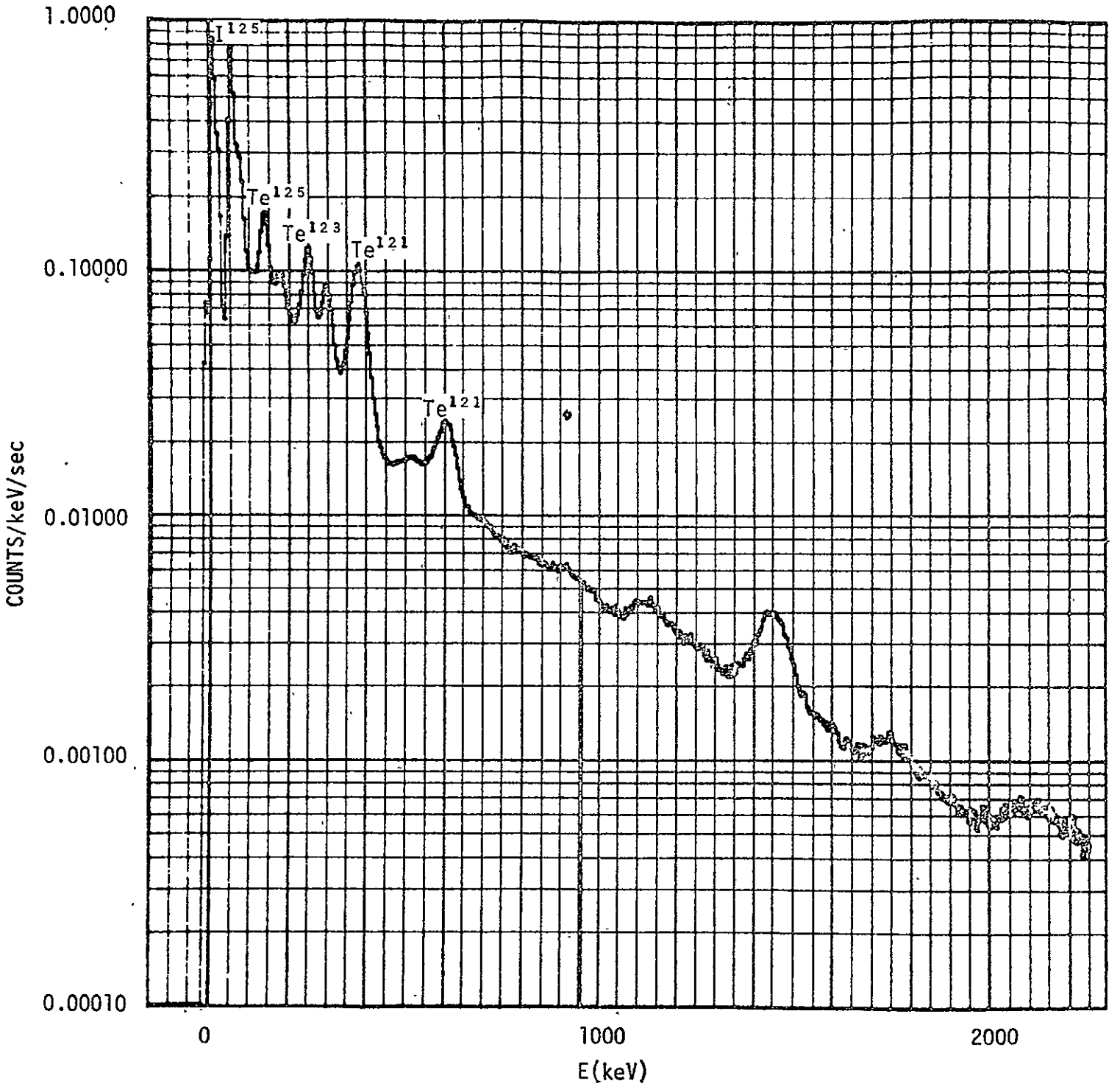

FIGURE B-12. SPECTRUM NUMBER 10

APPENDIX C. TIME DECAY CURVES FOR 600 MeV PROTON IRRADIATED NaI(Tℓ)

The counting rate as a function of time after irradiation is shown for each of five energy ranges. Generally, the decay follows a $1/t$ function which flattens prior to the 0.1 day and becomes steeper after 10^2 days. Counting rates in the 2- to 3-MeV energy range could not be taken after 10 days after irradiation because of experimental difficulties.

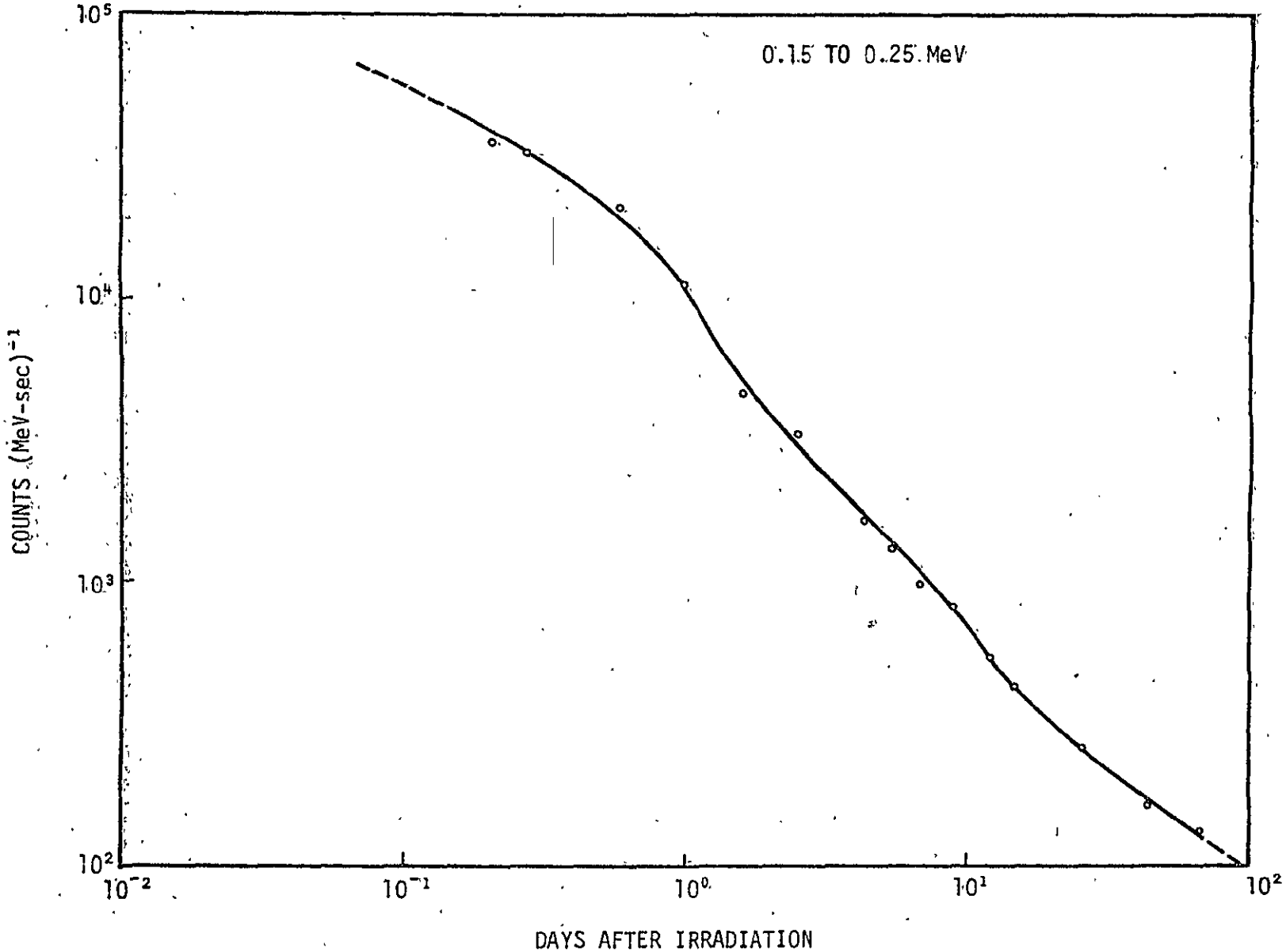

FIGURE C-1. COUNTING RATE AS A FUNCTION OF TIME AFTER IRRADIATION, RANGE 0.15 TO 0.25 MeV

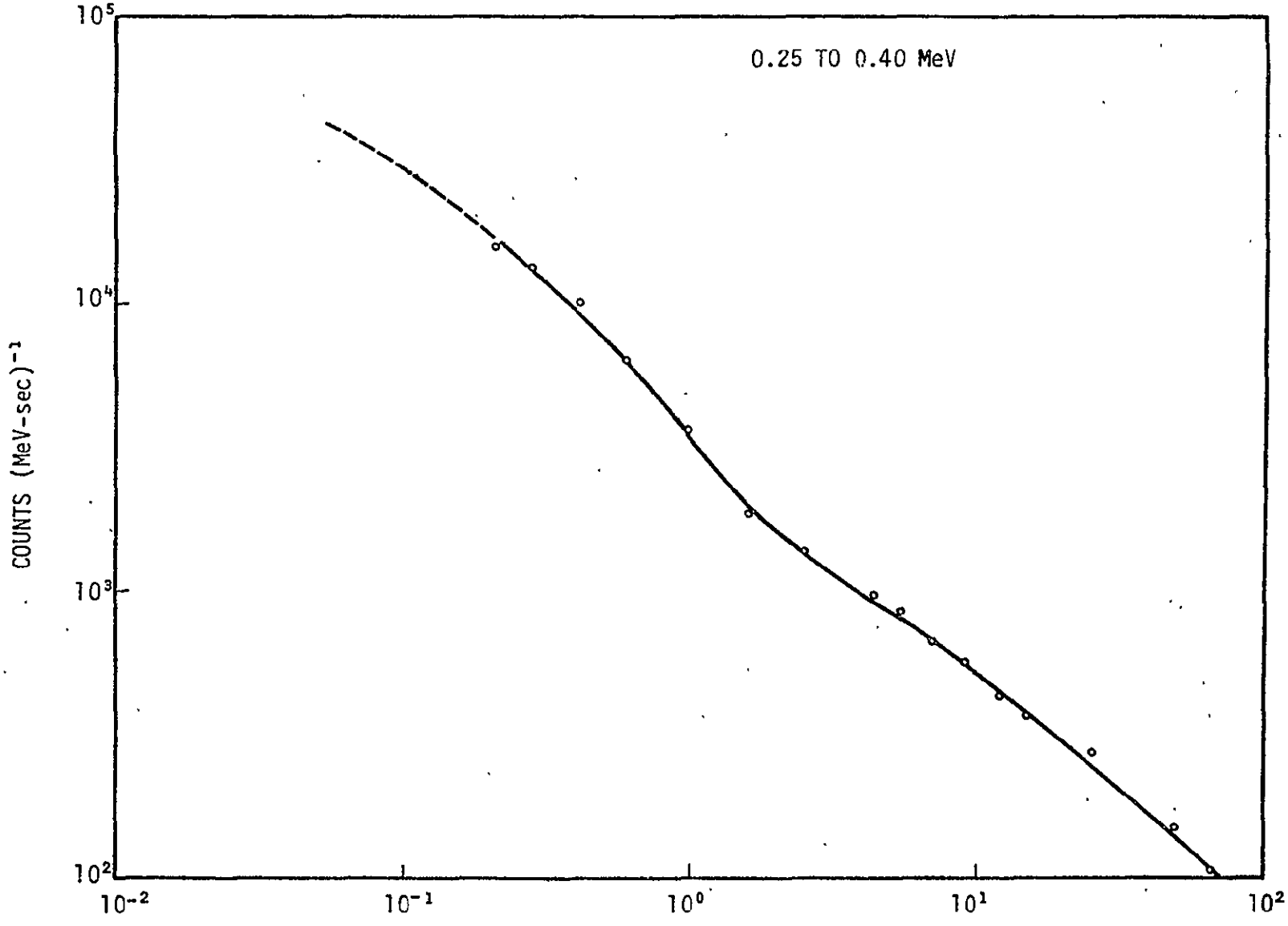

FIGURE C-2. COUNTING RATE AS A FUNCTION OF TIME AFTER IRRADIATION, RANGE 0.25 TO 0.40 MeV

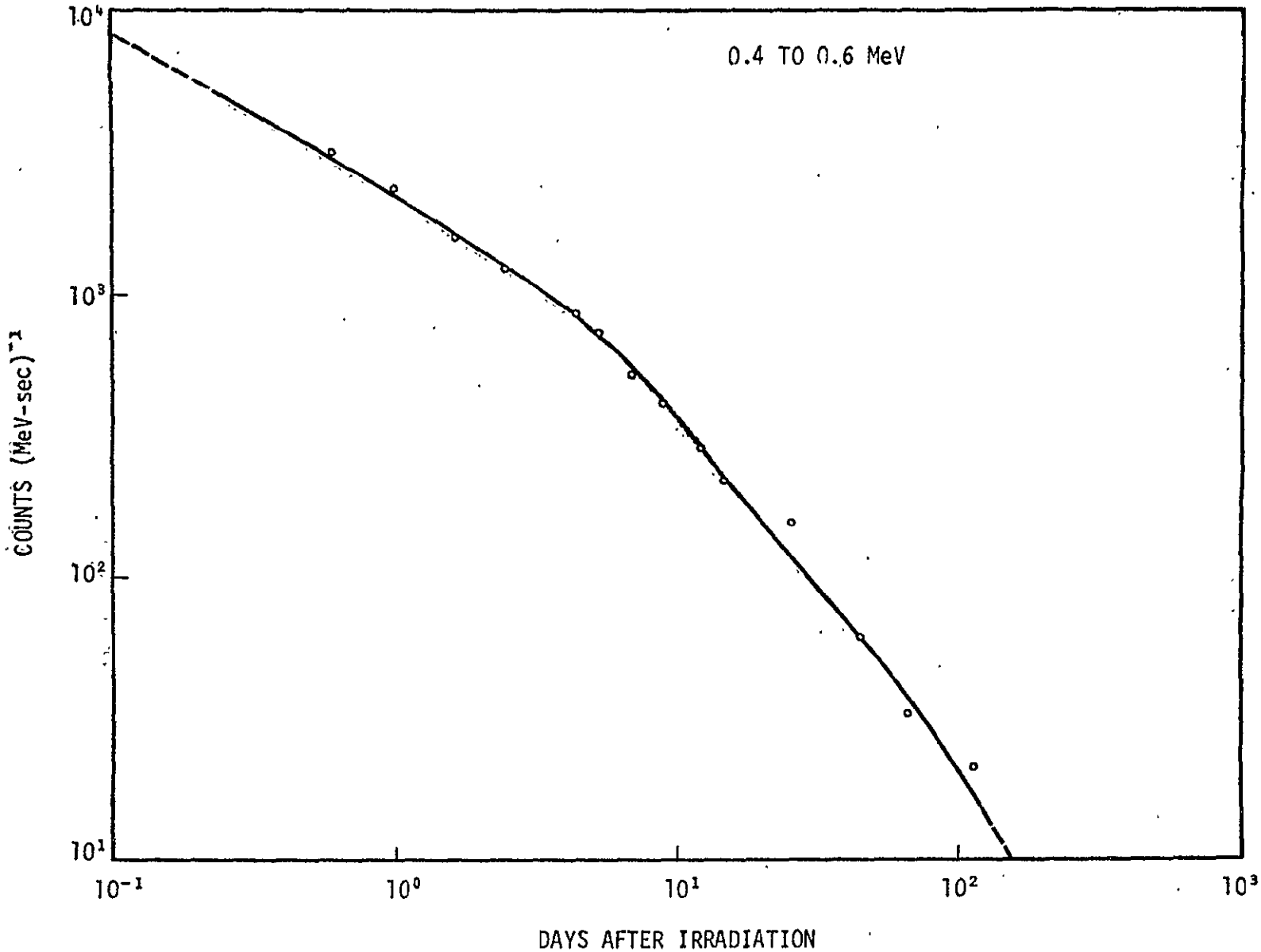

FIGURE C-3. COUNTING RATE AS A FUNCTION OF TIME AFTER IRRADIATION, RANGE 0.4 TO 0.6 MeV

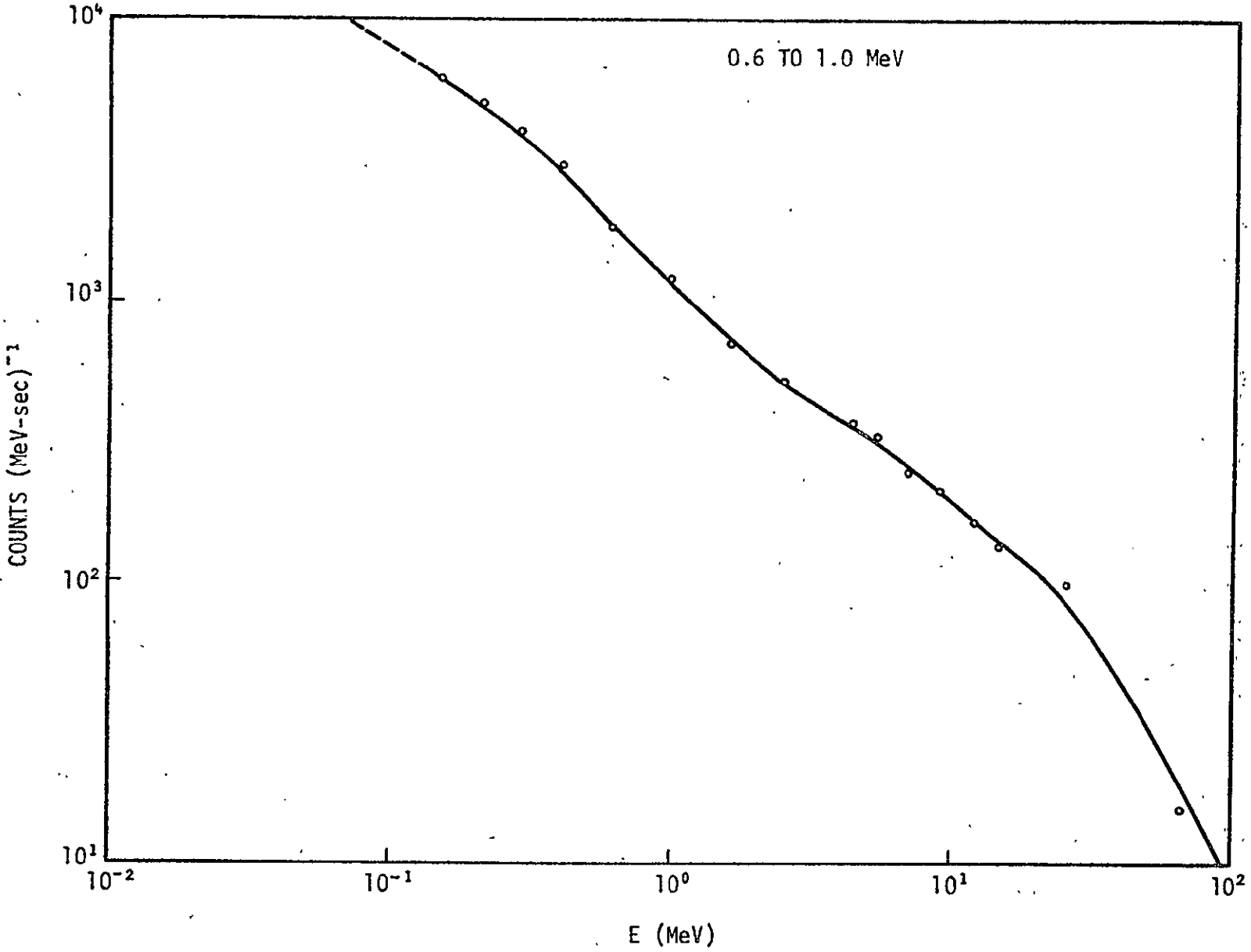

FIGURE C-4: COUNTING RATE AS A FUNCTION OF TIME AFTER IRRADIATION, RANGE 0.6 TO 1.0 MeV

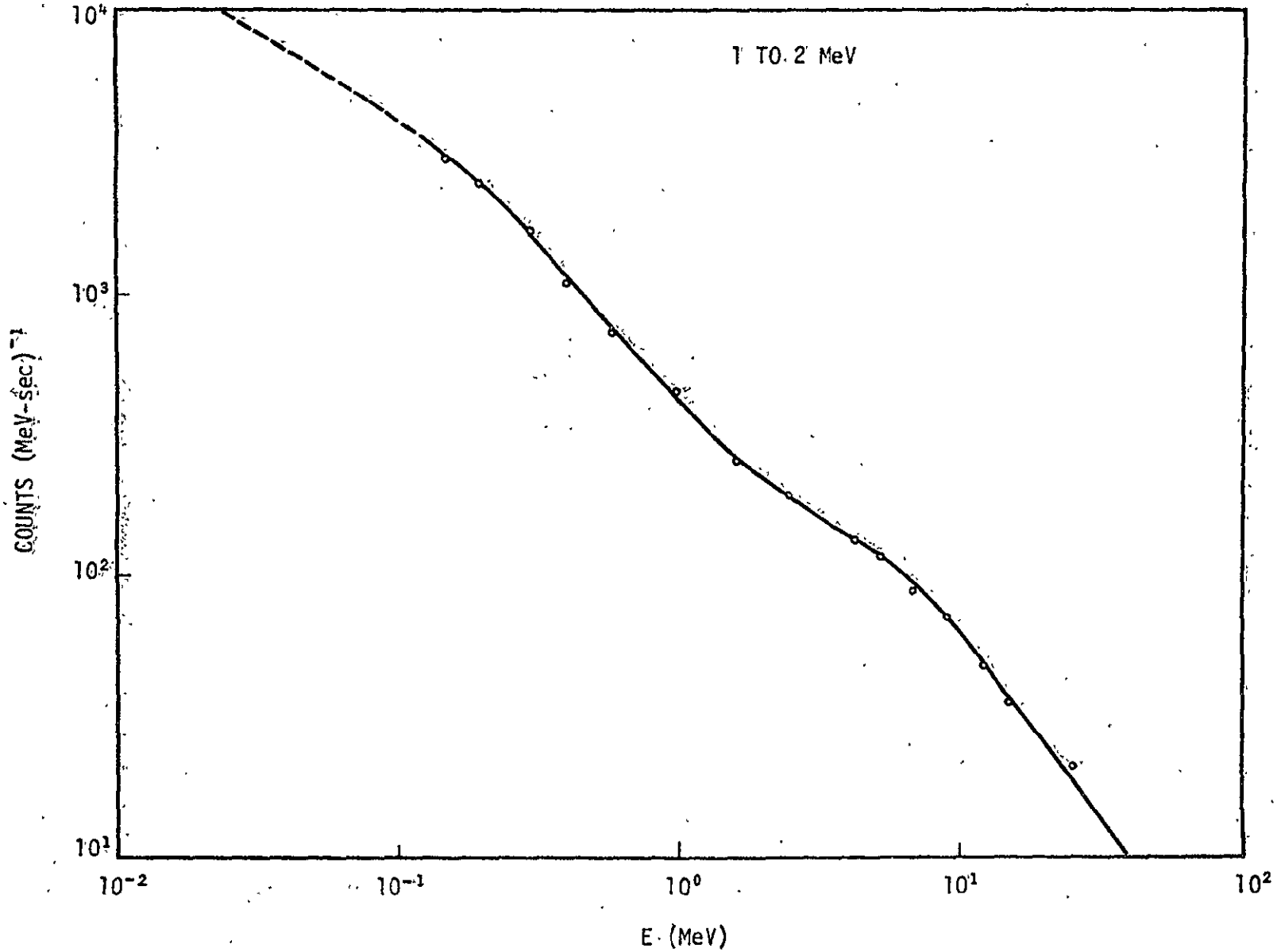

FIGURE C-5. COUNTING RATE AS A FUNCTION OF TIME AFTER IRRADIATION, RANGE 1 TO 2 MeV

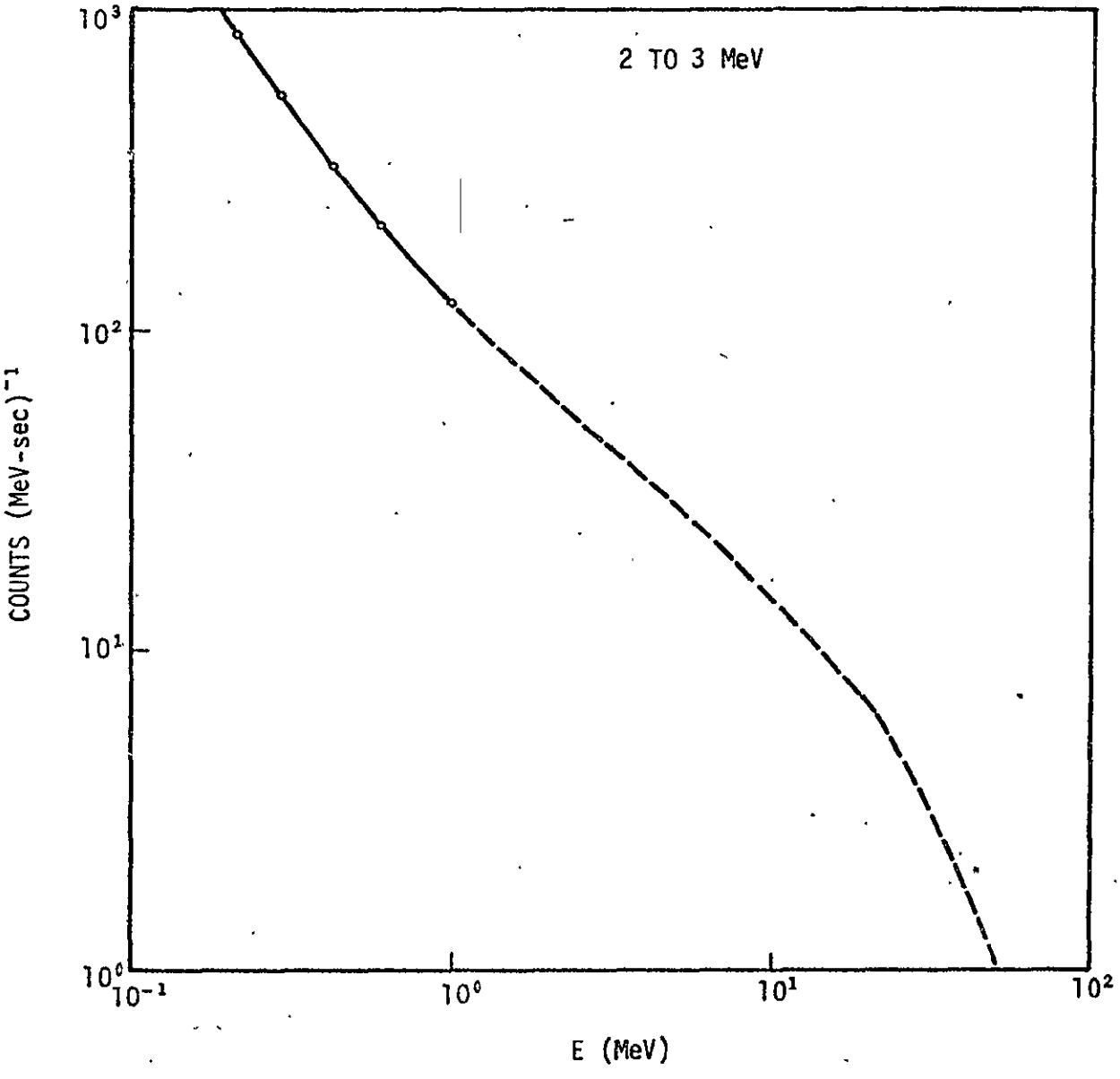

FIGURE C-6. COUNTING RATE AS A FUNCTION OF TIME AFTER IRRADIATION, RANGE 2 TO 3 MeV